University of Nebraska - Lincoln

# DigitalCommons@University of Nebraska - Lincoln

US Department of Energy Publications

U.S. Department of Energy

2007

# Cation exchange reactions controlling desorption of 90Sr2+ from coarse-grained contaminated sediments at the Hanford site, Washington

James Mckinley
*Pacific Northwest National Laboratory*, james.mckinley@pnl.gov

John M. Zachara
*Pacific Northwest National Laboratory*, john.zachara@pnl.gov

Steven Smith
*Pacific Northwest National Laboratory*, steven.smith@pnl.gov

Chongxuan Liu
*Pacific Northwest National Laboratory*, chongxuan.liu@pnl.gov

Follow this and additional works at: https://digitalcommons.unl.edu/usdoepub

Part of the Bioresource and Agricultural Engineering Commons

Mckinley, James; Zachara, John M.; Smith, Steven; and Liu, Chongxuan, "Cation exchange reactions controlling desorption of 90Sr2+ from coarse-grained contaminated sediments at the Hanford site, Washington" (2007). *US Department of Energy Publications*. 259.
https://digitalcommons.unl.edu/usdoepub/259

ELSEVIER

# Cation exchange reactions controlling desorption of $^{90}Sr^{2+}$ from coarse-grained contaminated sediments at the Hanford site, Washington

J.P. McKinley \*, J.M. Zachara, S.C. Smith, C. Liu

*Pacific Northwest National Laboratory, P.O. Box 999, Richland, Washington, USA*

## Abstract

Nuclear waste that bore $^{90}Sr^{2+}$ was accidentally leaked into the vadose zone at the Hanford site, and was immobilized at relatively shallow depths in sediments containing little apparent clay or silt-sized components. $Sr^{2+}$, $^{90}Sr^{2+}$, $Mg^{2+}$, and $Ca^{2+}$ was desorbed and total inorganic carbon concentration was monitored during the equilibration of this sediment with varying concentrations of $Na^+$, $Ca^{2+}$. A cation exchange model previously developed for similar sediments was applied to these results as a predictor of final solution compositions. The model included binary exchange reactions for the four operant cations and an equilibrium dissolution/precipitation reaction for calcite. The model successfully predicted the desorption data. The contaminated sediment was also examined using digital autoradiography, a sensitive tool for imaging the distribution of radioactivity. The exchanger phase containing $^{90}Sr$ was found to consist of smectite formed from weathering of mesostasis glass in basaltic lithic fragments. These clasts are a significant component of Hanford formation sands. The relatively small but significant cation exchange capacity of these sediments was thus a consequence of reaction with physically sequestered clays in sediment that contained essentially no fine-grained material. The nature of this exchange component explained the relatively slow (scale of days) evolution of desorption solutions. The experimental and model results indicated that there is little risk of migration of $^{90}Sr^{2+}$ to the water table.
© 2006 Elsevier Inc. All rights reserved.

## 1. Introduction

$^{90}Sr$ is a health hazard; it substitutes for Ca in bone (approximately 20% is retained after ingestion), and is responsible for bone cancer, soft-tissue cancers near bone, and leukemia. With a half-life of 28.78 years, it is a fission product from nuclear reactors and nuclear weapons, and the predominant Sr isotope. $^{90}Sr$ is a significant component of radionuclide contaminants at US Department of Energy sites, occurring in over half of those facilities nationwide (Riley and Zachara, 1992), where it was accidentally released. It was widely dispersed in the southwestern United States and elsewhere during the era of open-air nuclear weapons tests, and approximately 10 Pbq of $^{90}Sr$ was released by the nuclear accident at Chernobyl (OECD, 2002).

Chemically, Sr behaves much like Ca. They are both alkaline earths, exist in solution as divalent cations, and are of similar ionic radius (10 and 11.2 Å for Ca and Sr, respectively) (Rimstidt et al., 1998). Calcium has a continental crustal abundance of 50,000 mg kg$^{-1}$, and the calcium carbonate minerals are ubiquitous. Sr readily substitutes for Ca in calcite, $CaCO_3$ (Mucci and Morse, 1983; Stumm and Morgan, 1996), and it substitutes in the calcite polymorph, aragonite, to about one mole percent (Casey et al., 1996). Although $Sr^{2+}$ is not readily sorbed to the calcite surface (Zachara et al., 1991; Parkman et al., 1998), the $Sr^{2+}$ coprecipitation process progresses from binding of the less abundant $Sr^{2+}$ (continental crustal abundance 360 mg kg$^{-1}$) on the calcite surface, followed by calcite mineral overgrowth. Since the surfaces of the calcium carbonate minerals are reactive, they may continuously undergo surface precipitation-dissolution reactions with dissolved $Ca^{2+}$ and $HCO_3^-$, as evidenced by experimentation with calcite in the presence of solutions containing

---

\* Corresponding author.
*E-mail address:* james.mckinley@pnl.gov (J.P. McKinley).

$Ca^{2+}$ and $Sr^{2+}$ (Parkman et al., 1998). The interaction of solute ions to precipitate or dissolve calcite from groundwater could therefore directly affect the aqueous concentration of $Sr^{2+}$ and limit its mobility through coprecipitation. The natural coprecipitation of Sr with Ca has been confirmed in field studies of calcites, where coprecipitated $Sr^{2+}$ showed variation in solid phase concentrations in single populations, directly demonstrating its immobilization during migration in carbonate-bearing terrains (Ali, 1995; Vaniman and Chipera, 1996; Wogelius et al., 1997).

In surface interactions such as cation exchange on minerals other than calcite, $Sr^{2+}$ and $Ca^{2+}$ are chemical analogues (Lefevre et al., 1996; Parkman et al., 1998; Chitra et al., 1999). The surface complexation of cations to fixed-charge and amphoteric sites on mineral surfaces is a competitive reaction dependent upon surface site concentration, surface charge, and relative solute concentrations. A large aqueous concentration contrast between the $Sr^{2+}$ and more abundant $Ca^{2+}$ could influence the sorptive immobilization of $^{90}Sr^{2+}$ in groundwater systems, but even in the presence of significant $Ca^{2+}$, sorption and cation exchange have been shown to have significant effects on $Sr^{2+}$ concentrations in experimental mineral and sediment systems (Yanagi et al., 1989; Ohnuki and Kozai, 1994; Ahmad, 1995; Liu et al., 1995; Yasuda et al., 1995; Lefevre et al., 1996; Parkman et al., 1998; Strelko et al., 1998; Chitra et al., 1999).

Due to the presence and predominance of $Ca^{2+}$ in natural environments, and the chemical similarity of $Ca^{2+}$ and $Sr^{2+}$, an investigation of $^{90}Sr^{2+}$ as a contaminant must first include an evaluation of the behavior of $Ca^{2+}$, and the $Sr^{2+}$ ion may then be treated as a direct analogue. As implied above, the mobility of $Ca^{2+}$ is controlled by two major components in natural systems: the dissolution-precipitation (solubility) processes of $CaCO_3$ and $Ca^{2+}$ cation exchange on fixed charge sites, predominantly the exchange sites on aluminosilicate clay minerals such as the smectites. A review of groundwater flowpath studies where calcite was present and where waters achieved saturation with respect to calcite illustrates the interplay of carbonate mineral reactions and cation exchange. In some studied systems, carbonate mineral dissolution along the groundwater flowpath was reflected by increasing $Ca^{2+}$ concentrations (Langmuir, 1971; Smith and Drever, 1976; Zhu and Burden, 2001). Where calcite dissolution provided $Ca^{2+}$ to groundwater at recharge, followed by cation exchange down gradient, water quality progressively shifted to a composition dominated by $Na^+$ (Adams et al., 2001). In systems where the solubility reaction was not physically separated from cation exchange processes, cation exchange and mineral dissolution or precipitation occurred simultaneously, but the relationship was often not neatly resolved, due to ambiguities in data interpretation (Langmuir, 1971; DeSimone et al., 1997; Zhu and Burden, 2001; Naqa and Kuisi, 2004; Yamanaka et al., 2005). Field studies of $Sr^{2+}$ mobility confirmed that the aqueous concentration and movement of $Sr^{2+}$ was controlled by the presence of

$Ca^{2+}$, a function of calcite solubility and cation exchange (Magaritz et al., 1990; Lefevre et al., 1993, 1996; Vaniman and Chipera, 1996). In each case, observable $Sr^{2+}$ concentrations were attributable to processes controlling $Ca^{2+}$.

The Hanford site, in Washington State, was a component of the U.S. nuclear weapons complex beginning in 1943 and continuing until 1989. The processing of irradiated reactor fuel created huge volumes of radioactive wastes that were disposed by storage in underground tanks arranged in clusters, or 'farms.' The B farm of twelve tanks, beneath which the $^{90}Sr^{2+}$ plume we studied was located, was put into use in 1948 (Knepp, 2002). The buried, steel-lined, single-shell concrete tanks were built with individual capacities of 2000 $m^3$. They were used for over 40 years, but have been drained. Over several decades, numerous leak events (including near-surface liquid transfer leaks) occurred at the B farm (Corbin et al., 2001), and a plume of radioactive waste was entrained in the underlying vadose sediments. The composition of the waste varied, but all of the waste solutions contained sodium at concentrations of 1–3 mol $L^{-1}$. The BX-102 tank, for example, from which 347,000 L of waste leaked during tank-to-tank cascading operations in 1951, contained waste estimated to include 2.92 mol $L^{-1}$ $Na^+$ and 0.013 mol $L^{-1}$ $Ca^{2+}$ at pH 10.5, with no reported $Mg^{2+}$, $Sr^{2+}$, or $^{90}Sr^{2+}$ (Jones et al., 2001; Serne et al., 2003). Tank BX-101, which lost 15,000 L in 1972 during a liquid transfer accident, contained waste estimated to include 1.36 mol $L^{-1}$ $Na^+$, 0.009 mol $L^{-1}$ $Ca^{2+}$, no reported $Mg^{2+}$ or $Sr^{2+}$, and 0.045 Ci $L^{-1}$ $^{90}Sr^{2+}$ (Jones et al., 2001). The effects of tank leaks extended well into the vadose zone (Serne et al., 2002b), as indicated by the results of sediment extractions (Fig. 1).

## 2. Methods

We investigated the mineral residence of $^{90}Sr^{2+}$ that had leaked from a nuclear waste storage tank at the DOE Hanford site. In the sediments we studied, the solid-phase concentrations of $^{90}Sr^{2+}$ were low, so we examined the response of the contaminated sediments to desorption by varying concentrations of surface-competitive cations, and used microcharacterization techniques to determine its mineralogic residence. A leak from a transfer line sometime in the late 1960s to early 1970s released fluoride and carbonate along with sodium and $^{90}Sr^{2+}$ to the thick vadose zone. The waste moved laterally and vertically toward the water table at a depth of 78 m, but $^{90}Sr^{2+}$ was immobilized and confined to relatively shallow depths. The underlying sediment had been impacted by $NaHCO_3$-bearing solutions, so that the native $Ca^{2+}$ and $Sr^{2+}$ on the cation exchanger had been essentially completely replaced by $Na^+$. There was also a significant intrinsic $Sr^{2+}$ component to the carbonate minerals in place before introduction of the $^{90}Sr^{2+}$. We were thus provided with a system in which we could use the waste and natural components to
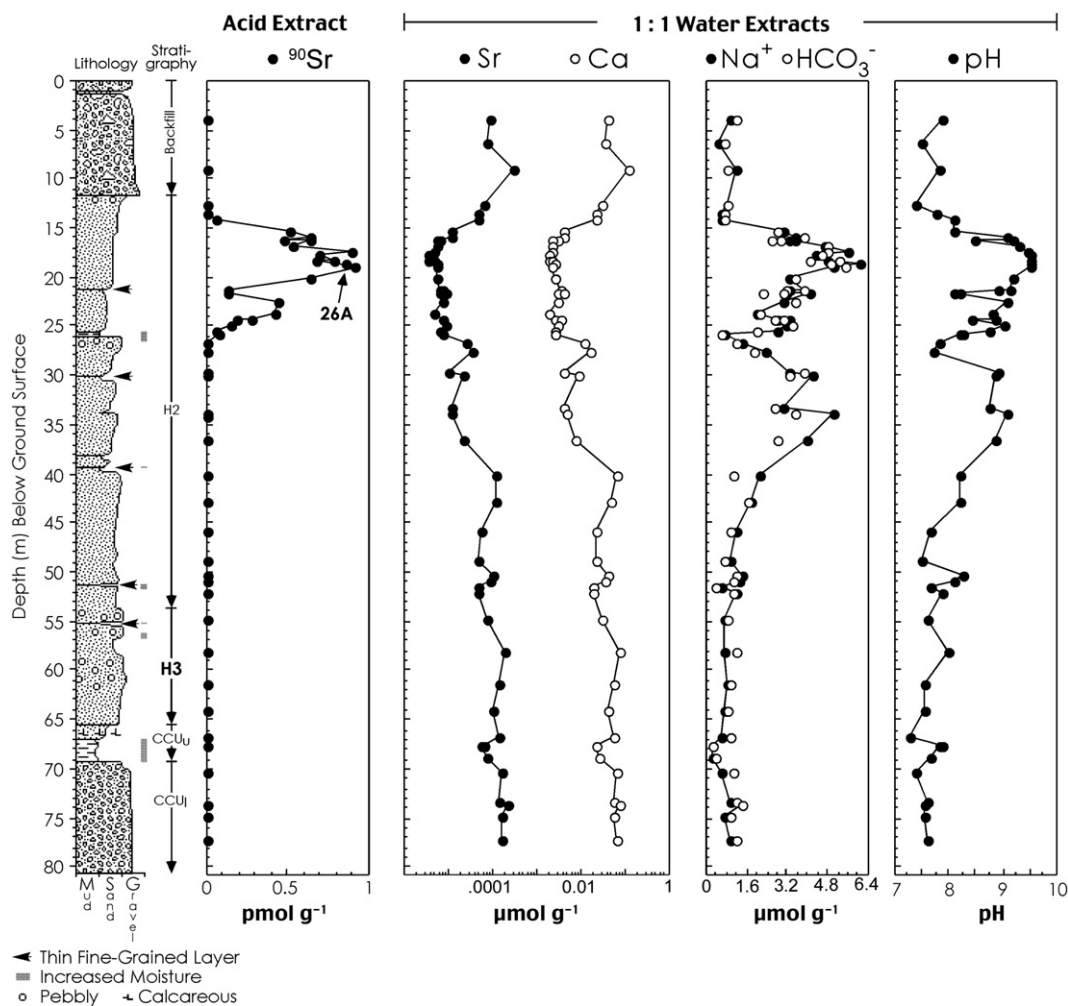
Fig. 1. Stratigraphy, acid extractable $^{90}Sr^{2+}$, and selected leachable cations.

determine the relative influence of carbonate solubility and cation exchange on the mobility of $^{90}Sr^{2+}$.

We used a suite of sampling and analysis methods. These included wet chemical techniques, such as batch desorption in electrolytes of different cation composition, and more spatially resolved techniques, such as electron microscopy and micro-autoradiography. The combined results of these methods culminated in the construction of a cation exchange model that explicitly included the contributions of calcium carbonate dissolution, which could fully explain the experimental results, and provided valuable information regarding the fate of $^{90}Sr^{2+}$ at the Hanford site.

### 2.1. Sediments

The vadose zone plume of $^{90}Sr$-bearing tank wastes was sampled by core drilling proximate to high-level waste tank B-110 in Hanford's B Tank Farm, from the ground surface to the water table. The drilling used the cable tool method, providing samples with minimal disturbance and without the use of drilling fluids. Four-inch diameter, two-foot split-spoon core samples were collected beginning at a depth of 3 m and continuing to 78 m, 2 m below the water table. Cores were extracted from half-foot core barrel liners in a radiologically controlled laboratory and sub samples were homogenized for geochemical analysis (Serne et al., 2002a).

Moisture contents were measured gravimetrically (ASTM, 1998).

Pore water composition was determined in two ways. Moisture contents were low (4–6 wt%), precluding the expression of pore waters from most samples. For a small number of samples, ultracentrifugation (Conca and Wright, 1998) was successful in producing aqueous samples of a few milliliters for compositional analysis. For most samples, ultracentrifugation was not successful, and an attempt was made to determine pore water solute compositions using a modification of the procedure for determining soil salinity (Rhoades, 1996). A representative sediment subsample of 15–70 g was combined with a mass of deionized water that would, based on moisture content, yield a 1:1 mass ratio of sediment to water. This mixture was shaken for one hour, then the supernatant removed and analyzed

directly for pH, and filtered (0.45 μm) for other analyses. Solute concentrations were determined using standard methods for dissolved cations (EPA, 2000a,b), anions (EPA, 1984), and alkalinity (USGS, 2001). Results for all analytes were tabulated and published elsewhere (Serne et al., 2002a).

## 2.2. Desorption measurements

For the $^{90}$Sr desorption experiments, approximately 2.0 g of air-dried sediment from the borehole at the B tank farm designated 299-E33-46 was weighed into polycarbonate centrifuge tubes and 4.0 mL of solution were added to each tube. Eight desorption electrolytes were used: deionized water, 0.01 mol $L^{-1}$ NaNO$_3$, 0.05 mol $L^{-1}$ Ca(NO$_3$)$_2$, 1 mol $L^{-1}$ NaNO$_3$, 1 mol $L^{-1}$ Na acetate (NaOAc) at pH 5.0, 5.0 mol$^{-1}$ L NaNO$_3$, 0.5 mol $L^{-1}$ HCl, and 1 mol $L^{-1}$ NH$_4$Cl. For a subset of electrolytes (0.05 mol $L^{-1}$ Ca(NO$_3$)$_2$, 1 mol $L^{-1}$ NaNO$_3$, and 5.0 mol$^{-1}$ L NaNO$_3$), the experiments were repeated after the sediment was washed three times (again, 2 g sediment/4.0 mL H$_2$O) for two hours each time in deionized water to remove soluble carbonate, then dried. Washing was expected to have three potential consequences: it would remove residual solutes, particularly bicarbonate, and prevent their reaction with desorbed solutes during leaching; it could remove soluble solid phases, such as sodium bicarbonate, that might have precipitated during or after exposure to waste solutions; and it could change the behavior of the exchange system by modifying the exchanger phase composition. The tubes were placed in a horizontal position in an incubator shaker set at 60 cycles per minute and 25 °C for continuous mixing through 7 days. After seven days, the suspensions were mixed by hand daily. Single tubes of each solution were sampled at 30 min, 2, 4, 8, 24 h, 2, 4, 7, 14, 21, and 28 days. The solution sample was obtained by centrifuging the tubes for 15 min at 5000 rcf. One milliliter of the clear supernatant was transferred to a polycarbonate tube containing 9 mL deionized water. The diluted sample was filtered using a 10 mL plastic syringe fitted with a 0.2 μm filter. The first 1 mL of filtrate was discarded and the remainder collected in a polystyrene tube. At every other sampling event (i.e., 0.5, 4, 24 h, 4, 14, and 28 days) a portion of the filtrate was collected in a 4 mL glass, septum-capped vial for determination of dissolved inorganic carbon and a separate portion was analyzed as above (EPA, 2000b) for barium, calcium, chromium, potassium, magnesium, strontium, and sodium, and the pH was determined for the other suspensions.

Bulk $^{90}$Sr concentrations were determined by leaching with 8 mol $L^{-1}$ nitric acid (liquid/solid = 5:1, mass ratio) for several hours at 80 °C, followed by centrifugation and 0.2 μm filtration.

$^{90}$Sr was quantitated by liquid scintillation counting. The $^{90}$Sr/$^{90}$Y activity in the solution phase was determined within a counting window of 0 to 2000 keV. Since the isotopes co-exist in equilibrium after 28 days, the total activity was counted 28 days after sampling, and a quench curve yielded twice the true $^{90}$Sr activity.

## 2.3. Digital autoradiography and scanning electron microscopy

Digital autoradiography was used to determine $^{90}$Sr distribution in bulk sediments and its intraclast distribution in thin sections. The phosphor imaging system consisted of a Fujifilm BAS-5000 scanner set for 16 bit, 25μm pixel digitization and phosphor plates (BAS TR-2025) sensitive to ionizing radiation. Exposures were made within a cave of lead bricks to reduce background radiation levels. The digital readout in this system is in units of photo-stimulated luminescence (PSL), arbitrarily set and calibrated by the manufacturer against a standard $^{14}$C source for consistency between instruments and identically treated samples. The correlation of PSL units to activity is dependent in part on the efficiency of the phosphor plate in capturing and detecting radiation of differing energies. The instrument is sensitive to all radiation, however, and has been used to image radiation from a variety of sources (Zeissler et al., 1998). It can be used at very low activity levels. Parallel autoradiography and γ counting of individual mica flakes contaminated with $^{137}$Cs showed a linear correlation of PSL units and activity to a lower level of 0.0007 Bq (Zeissler et al., 2001). For digital autoradiography, Sr-contaminated sediments were prepared in two ways. For screening of bulk sediments, loose sediment grains were scattered onto glass slides and affixed with collodion. For intraclast analysis of $^{90}$Sr distribution, sediments were imbedded in epoxy resin, wafered, affixed to fused quartz slides (which provide a low background), and ground and polished to a thickness of approximately 100 μm.

Thin-sectioned samples were imaged for mineralogic information using a JEOL 6340 field emission Scanning electron microscope (SEM), using a backscattered electron (BSE) detector to provide atomic number contrast. Elemental abundances were determined using a JEOL 8200 electron microprobe. Individual spectrometers were tuned to Na, K, Ca, and Mg Kα X-radiation, and the intensity of emitted radiation was recorded as the sample was moved under the 20 keV, 20 nA electron beam, with 1 μm steps at a dwell of 500 ms. The auto-scaled false-color spectra were in a 'rainbow' motif, with red equivalent to maximum abundance. Electron microprobe analyses were collected against mineral standards, and corrected using a ZAF routine. Autoradiography and BSE images were merged using Adobe Photoshop.

## 3. Results

### 3.1. Sediment pore waters

Under centrifugation, eight of the sixty core samples yielded sufficient pore water for compositional analysis

(Table 1). Processing 150 g of sediment yielded about 2–3 mL of pore water, which was divided and diluted as necessary for analysis. Equilibrium thermodynamic modeling (Allison et al., 1991) of the expressed compositions was used to calculate the saturation index (SI), defined as the log (IAP/$K$), where IAP was the ion activity product of the components of the mineral of interest, and $K$ was its solubility constant. The solutions were within approximately 0.5 log units of saturation with respect to aragonite, which is often observed as the initial calcium carbonate mineral in aqueous systems reaching saturation (Stumm and Morgan, 1996); the calcite SI was offset from the aragonite values by a constant of +0.13. The SI for aragonite, more soluble than calcite, represented a convenient reference for the solution compositions, but the use of aragonite indices was not meant to imply that that was the carbonate phase present in the samples studied: in evaluations of sediment pore waters we used aragonite SI values for discussion purposes, and for other results we used calcite, the likely solid phase in the pristine sediment, as a reference. Analysis of the sediments by X-ray diffraction (Serne et al., 2002b) did not indicate the presence of $CaCO_3$. Compositional analysis, however, showed an abundance for inorganic carbon of about 0.2 wt%, equivalent to about 1.6 wt% $CaCO_3$ (Serne et al., 2002b). In our results, the presence of a $CaCO_3$ phase was deduced from extraction data (below).

The calculated charge balance (C.B.) for the pore water analyses was within approximately 30% of neutral, where the C.B. = [(cation equivalents − anion equivalents)/(cation equivalents + anion equivalents)] × 100%. The major components of analysis—cations, anions, inorganic carbon, and pH—each represented independent analytical procedures on separate sample aliquots. Considering the

sample volumes available, the approach to charge balance from combining the results of disparate analytical procedures was reasonable. The SI was well correlated with pH ($r^2 = 0.85$), and the departure from an SI of zero for either aragonite or calcite likely resulted from the effects of sample processing on pH or on inorganic carbon concentrations. The potential effects of $Mg^{2+}$ substitution on $CaCO_3$ solubility were not evaluated, even though the extractions indicated a $CaCO_3$ phase with approximately 4 mole % $Mg^{2+}$ (discussed below). Previous work suggested that $Mg^{2+}$ substitution could have some solubility effect on calcite, but the effect would not be significant at $Mg^{2+}$ substitutions of less than 10% (MacKenzie et al., 1983; Mucci and Morse, 1983; Mucci and Morse, 1984; Stumm and Morgan, 1996), and would be indiscernible in our results.

Pore waters in the upper portion of the sediment column were compositionally distinct (Table 1). To a depth of 25 m (Sample 38a), $Na^+$ was abundant and present at 50–100 times $Ca^{2+}$; $HCO_3^-$ was at least twice as abundant as the sum of the other anions; and the pH was greater than 8. These compositions were consistent with the displacement of the original pore water by alkaline $NaHCO_3$ tank wastes. In contrast, the deepest sample, No. 113 at 68.9 m, included $Na^+$ at approximately twice the concentration of $Ca^{2+}$; had $HCO_3^-$ at a about one-third of the sum of the other anions; and was at circumneutral pH. This composition represented the undisturbed pore waters in the vadose sediments.

The 1:1 water leachate compositions (Fig. 1), plotted as the moles of analyte per gram of sediment, demonstrated the vertical extent of sediment interaction with waste solutions. The tank bottoms lay at a depth of 12 m, and the effects of the waste plume were detected within 2–3 m of that depth. Leachate $Na^+$ and $HCO_3^-$, the major waste

Table 1
Pore water compositions after centrifugation

| Sample No. | Depth (m) | Chge Bal. (%) | Cations (mmol L$^{-1}$) | | | | | |
|---|---|---|---|---|---|---|---|---|
| | | | $Ca^{2+}$ | $K^+$ | $Mg^{2+}$ | $Na^+$ | $Sr^{2+}$ | $H_4SiO_4{}^0$ |
| 20b | 15.3 | 28.6 | 0.168 | 0.700 | 0.070 | 8.174 | 0.000457 | 0.553 |
| 21a | 16.2 | 9.1 | 0.184 | 0.415 | 0.074 | 12.348 | 0.000457 | 0.490 |
| 36a | 24.4 | 12.2 | 0.182 | 0.541 | 0.086 | 10.609 | 0.000457 | 0.490 |
| 38a | 25.3 | 11.2 | 0.139 | 0.274 | 0.057 | 13.696 | 0.000342 | 0.550 |
| 84 | 51.4 | 12.6 | 2.168 | 0.541 | 1.189 | 7.435 | 0.005822 | 0.518 |
| 105c | 63.7 | −35.3 | 1.145 | 0.305 | 0.531 | 3.861 | 0.002854 | 0.728 |
| 110b | 67.6 | 16.5 | 2.825 | 0.374 | 1.313 | 5.174 | 0.007420 | 0.547 |
| 113 | 68.9 | 20.2 | 1.330 | 0.333 | 0.605 | 2.965 | 0.003539 | 0.447 |
| | pH | Aragonite SI | Anions (mmol/L) | | | | | |
| | | | $NO_3^-$ | $F^-$ | $Cl^-$ | $SO_4^{2-}$ | $PO_4^{2-}$ | $HCO_3^-$ |
| 20b | 8.23 | | 0.129 | 0.632 | 0.204 | 0.324 | 0.019 | 3.541 |
| 21a | 8.69 | 0.472 | 0.277 | 0.758 | 0.366 | 0.969 | 0.023 | 7.672 |
| 36a | 8.39 | 0.149 | 0.081 | 1.300 | 0.203 | 0.629 | 0.000 | 6.311 |
| 38a | 8.45 | 0.085 | 0.215 | 1.484 | 0.501 | 1.188 | 0.000 | 6.902 |
| 84 | 8.02 | 0.046 | 7.774 | 0.026 | 0.600 | 0.993 | 0.000 | 1.033 |
| 105c | 7.00 | −0.509 | 3.242 | 0.095 | 1.837 | 2.938 | 0.000 | 4.705 |
| 110b | 7.16 | −0.483 | 4.355 | 0.000 | 0.927 | 1.813 | 0.000 | 1.000 |
| 113 | 7.41 | −0.744 | 1.694 | 0.000 | 0.451 | 0.828 | 0.000 | 0.967 |

ions, defined a broad zone of waste–sediment interaction, with elevated $Na^+$ and $HCO_3^-$ persisting to a depth of approximately 50 m. Extractable $Sr^{2+}$ and $Ca^{2+}$ were displaced and flushed from the sediment column by waste $Na^+$, and were most affected over the interval from 15 to 27 m in depth, where water-extractable $Sr^{2+}$ was about 5 pmol $g^{-1}$ and $Ca^{2+}$ was about 1 nmol $g^{-1}$. The distribution of $^{90}Sr$ (determined by acid extraction; Fig. 1) was restricted to the 15–27 m interval where water leachable $Sr^{2+}$ and $Ca^{2+}$ were lowest, and the maximum $^{90}Sr^{2+}$ concentration was less than 1 pmol $g^{-1}$ at about 19 m in depth. Leachate solutions were alkaline, with pH above 8 over most of the affected depth interval.

The displacement of $Ca^{2+}$, $Mg^{2+}$, and $Sr^{2+}$ from exchanger sites during the intrusion of the $NaHCO_3$ tank waste may have caused the supersaturation and precipitation of calcium carbonate. The concentrations of $Na^+$ and $HCO_3^-$ in the waste solution were one order of magnitude larger, or more, than the pre-existing pore water concentrations (Table 1). The waste-induced transition from a condition of mixed-ion solutions in equilibrium with the exchanger phase and calcite, to a system where $Na^+$ predominated is shown schematically in Fig. 2. The original divalent pore water cations plus the cations displaced into solution by the relatively concentrated waste $Na^+$ reacted with waste $HCO_3^-$ to form $(Ca,Mg,Sr)CO_3$. Centrifuged

pore water from within the interval containing $^{90}Sr^{2+}$, such as from Sample 38a (Table 1), had charge balance and saturation indices near zero with respect to aragonite. The Sample 38a pore water solution included 0.14 mmol $L^{-1}$ $Ca^{2+}$ and 6.9 mmol $L^{-1}$ $HCO_3^-$, compared to 1.3 and 1.0 mmol $L^{-1}$, respectively, for the same ions in Sample 113 (Table 1). The difference in divalent cation concentrations between the two samples may have represented the precipitation of a carbonate phase. Also, the samples where $Ca^{2+}$ was depleted (samples above 51 m depth; Table 1) bracketed the interval where acid-leachable $^{90}Sr^{2+}$ was found, and it may be assumed that the $CaCO_3$ precipitated there included some co-precipitated $^{90}Sr$.

### 3.2. Sediment textures

The sediments most impacted by tank waste were coarse to medium sand, with little clay or silt, and were determined to belong to the H2 unit of the Hanford Formation, a deposit of Pleistocene epoch catastrophic flood debris. Within the clay-sized fraction, smectite, illite, and chlorite predominated (Serne et al., 2002b). Because the Hanford site is within the area underlain by voluminous Columbia River Flood Basalt, the H2 deposit includes abundant basaltic lithic fragments (Bjornstad, 1990; Reidel and Fecht, 1994). The center of the $^{90}Sr$ plume was within a
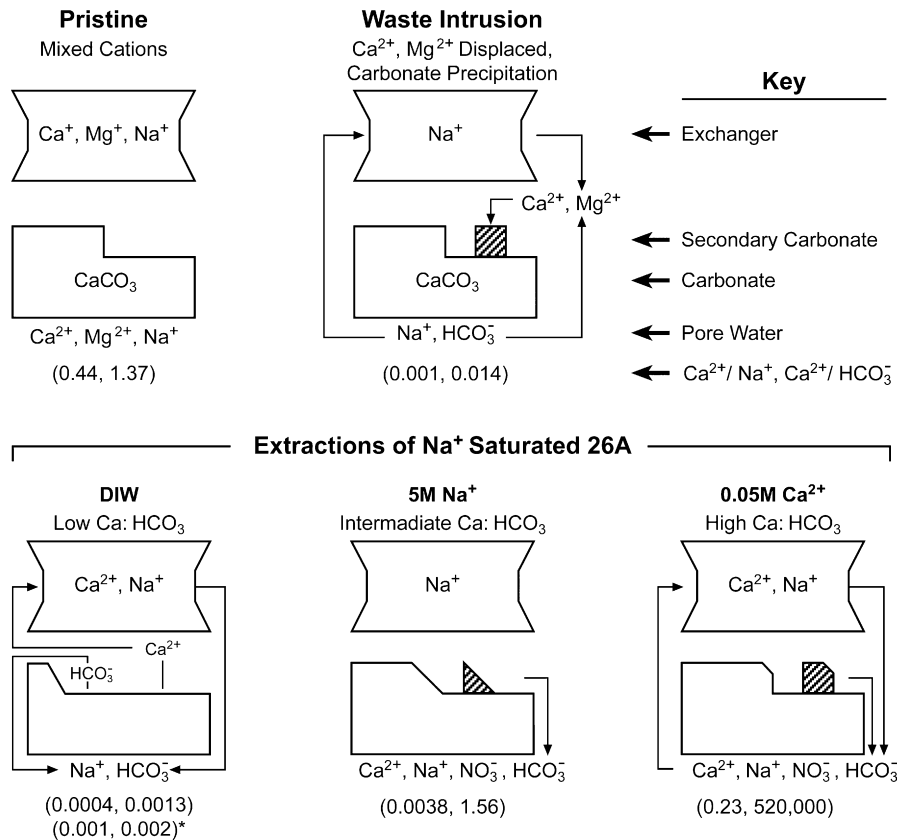


Fig. 2. Two component conceptual model of ion relationships in pristine sediment, waste-impacted sediment, and during extraction with deionized water, $Na^+$, and $Ca^{2+}$.

relatively homogeneous interval of coarse sand. Samples from within the interval containing $^{90}Sr$ (Fig. 1) were almost devoid of fines, including an average of 1.5 wt% clay-sized material (Serne et al., 2002a). In contrast, most other Hanford sediments, a relatively abundant phyllosilicate smectite fraction functions as the exchanger phase. A thin, fine-grained interval at a depth of approximately 21 m showed a markedly lower concentration of $^{90}Sr$ than its surroundings; it was apparently not well infiltrated during the migration of $^{90}Sr$-bearing waste.

## 3.3. Desorption experiments

For desorption studies, Sample 26A, with an activity of 388 Bq g$^{-1}$, from the center of the $^{90}Sr$ plume (Fig. 1), was used to represent the character and behavior of all, similar, H2 sediment. (An activity of 388 Bq g$^{-1}$ for $^{90}Sr$ is equivalent to $8.55 \times 10^{-13}$ mol g$^{-1}$, or 0.855 pmol g$^{-1}$. For comparisons with other ions, $^{90}Sr$ was expressed in molar units: 1 Bq $= 2.20 \times 10^{-15}$ mol). Desorption results from Sample 26A were represented as time-series extraction concentrations (Figs. 3–5). Extractant concentrations were approximately constant after seven days; the fourteen-day values thus provided a convenient point of comparison between experiments (Table 2). Where the values for solutes from 0.5 mol L$^{-1}$ HCl and 1 mol L$^{-1}$ NaOAc extractions

were large enough to obscure the differences between other extraction experiments, they were omitted from the figures, but their fourteen-day values were included in Table 2.

### 3.3.1. Strontium

Extraction solutions were formulated based on the results of other investigators (Serne et al., 2002a) and on Sr–Ca–Na ion exchange experiments with uncontaminated H2 sediments (Lichtner and Zachara, 2005), which showed negligible adsorption ($K_d = 0$) for $^{90}Sr^{2+}$ in 5 mol L$^{-1}$ NaNO$_3$, due to competitive mass action of the electrolyte cation. That solution was therefore considered to be a desorption electrolyte that would fully displace divalent cations sorbed to the exchanger phase. The amounts of $^{90}Sr^{2+}$ released in 0.5 mol L$^{-1}$ HCl and 1 mol L$^{-1}$ NaOAc at pH 5 were identical within a few percent (Table 2), and the extracted $^{90}Sr^{2+}$ (average 0.770 pmol $^{90}Sr^{2+}$ g$^{-1}$) was considered to be complete $^{90}Sr^{2+}$ extraction. Our desorption experiments (Fig. 3a) yielded no $^{90}Sr^{2+}$ release in deionized water or 0.01 mol L$^{-1}$ NaNO$_3$; approximately 50% $^{90}Sr^{2+}$ release in 1 mol L$^{-1}$ NaNO$_3$ and 0.05 mol L$^{-1}$ Ca(NO$_3$)$_2$; and 75% $^{90}Sr^{2+}$ release in 5 mol L$^{-1}$ NaNO$_3$.

The desorption/dissolution kinetics of the $^{90}Sr^{2+}$ and the stable strontium isotopes ($^TSr$) were similar. The concentrations of extracted $^{90}Sr^{2+}$ and $^TSr$ increased with the ionic strength of the extracting solutions (e.g., the
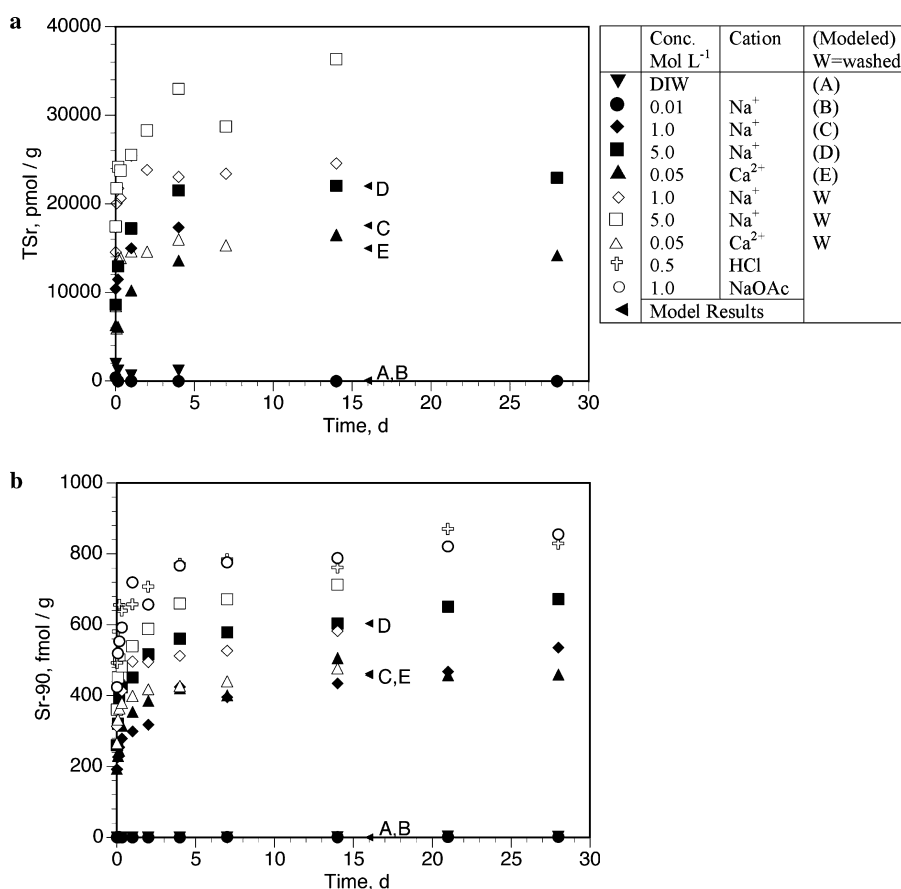
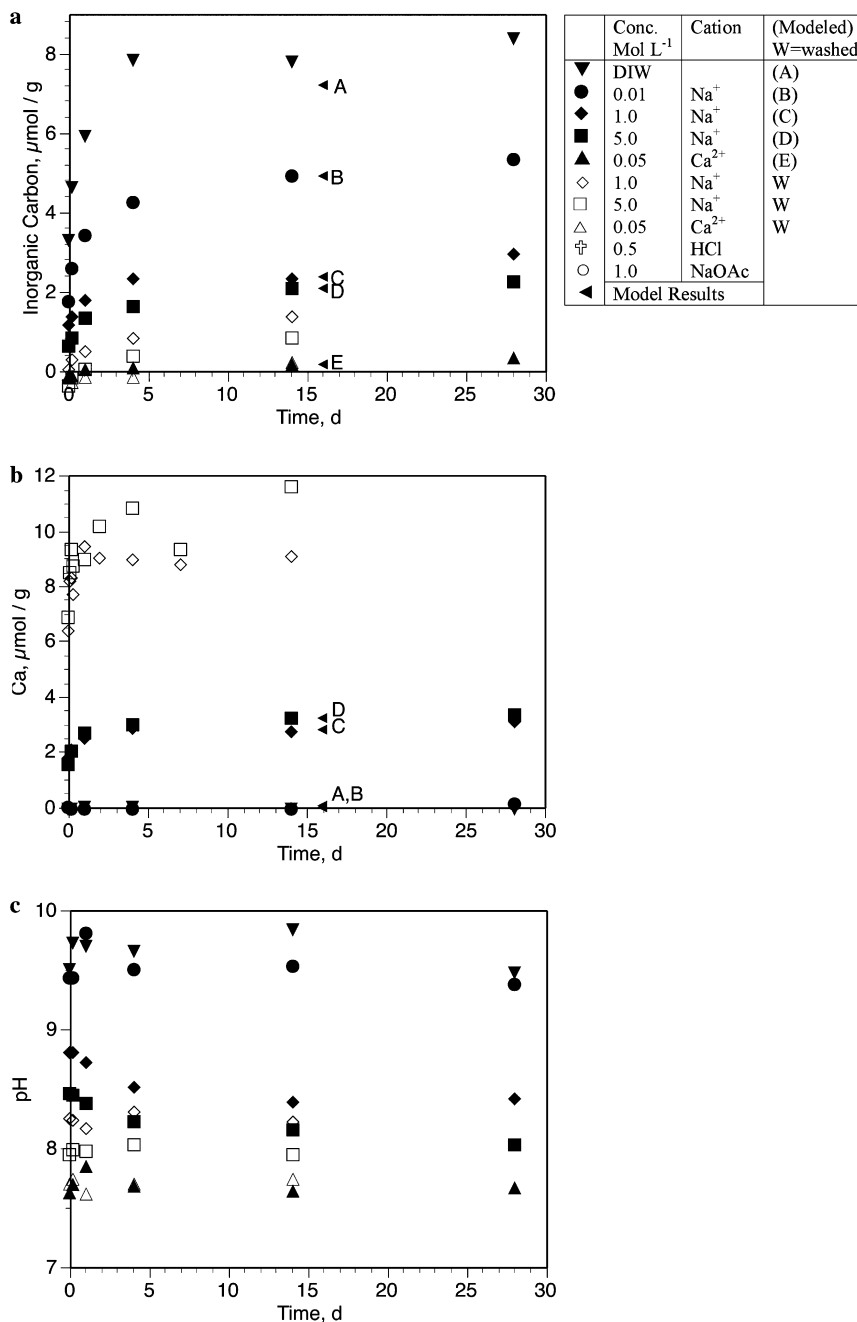Fig. 3. Extraction data for $^TSr^{2+}$ and $^{90}Sr^{2+}$, exchange model results shown.

Fig. 4. Extraction data for $Ca^{2+}$, $HCO_3^-$, and leachate pH, with exchange model results.

progression in increasing extracted concentration for both $^{90}Sr^{2+}$ and $^TSr$ for unwashed sediments was in the following order of extracting cations: deionized water, 0.01 mol $L^{-1}$ $Na^+$, 0.05 mol $L^{-1}$ $Ca^{2+}$, 1.0 mol $L^{-1}$ $Na^+$, 5 mol $L^{-1}$ $Na^+$, 0.5 mol $L^{-1}$ HCl and 1.0 mol $L^{-1}$ NaO-Ac; Table 2, Fig. 3a and b. The extraction behavior of HCl and NaOAc solutions did not fall on the same ionic strength trend as the other solutions). The results conformed to the expectation that $^TSr$ and $^{90}Sr^{2+}$ would be chemically associated on the solid phase and that they would behave identically during ion exchange. The ion-exchange relationship was consistent with the in-ground

attenuation of $^{90}Sr^{2+}$ (Fig. 1) by an exchange mechanism during contaminant migration.

The molar ratio of $^{90}Sr^{2+}$ to $^TSr$, ($^{90}Sr/^TSr$; Table 2), was lower when sediments were extracted with HCl or NaOAc ($^{90}Sr/^TSr = 5.3–5.5 \times 10^{-6}$) than when they were extracted with water or solutions of $Ca^{2+}$ or $Na^+$($^{90}Sr/^TSr = 20–30$ μmol $mol^{-1}$). This difference was due to the different behavior of the solid phase in the presence of the two types of extracting solution. Extraction using $Na^+$ and $Ca^{2+}$ would favor the removal of exchangeable $^{90}Sr^{2+}$ and $^TSr^{2+}$, while extraction with HCl and NaOAc would remove exchangeable $^{90}Sr^{2+}$ and $^TSr^{2+}$, $^{90}Sr^{2+}$ and $^TSr^{2+}$
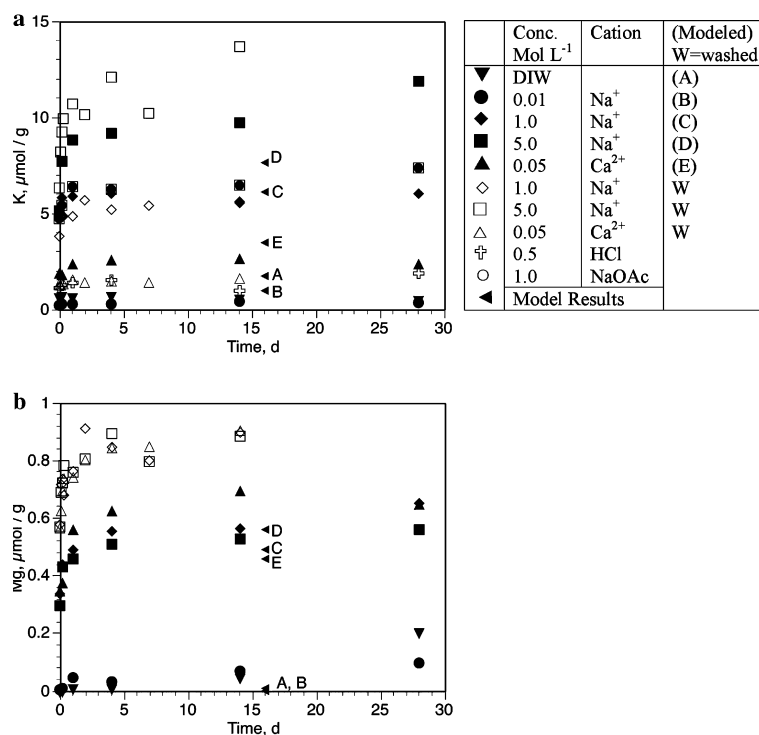
Fig. 5. Extraction data for $Mg^{2+}$ and $K^+$ with exchange model results.

Table 2
Leachate results after fourteen days, Sample 26A, for experiments using unwashed (-U), and washed (-W) sediments

| Leachate | pH | IC ($\mu$mol g$^{-1}$) | Ca ($\mu$mol g$^{-1}$) | Na ($\mu$mol g$^{-1}$) | K ($\mu$mol g$^{-1}$) | Mg ($\mu$mol g$^{-1}$) | $^T$Sr (pmol) | $^{90}$Sr (fmol) | $^{90}$Sr/$^T$Sr $\times 10^6$ | Calcite SI |
|---|---|---|---|---|---|---|---|---|---|---|
| DIW | 9.84 | 7.81 | 0.01 | 25.5 | 0.51 | 0.04 | *1000* | 1 | — | −0.41 |
| 0.01 Na-U | 9.53 | 4.93 | 0.01 | — | 0.44 | 0.07 | −2000 | 1 | — | |
| 0.05 Ca-U | 7.65 | 0.19 | — | 36.3 | 2.67 | 0.70 | 16,000 | 506 | 31.6 | |
| 1.0 Na-U | 8.40 | 2.37 | 2.79 | — | 5.64 | 0.57 | *17,000* | 435 | 25.6 | −0.25 |
| 5.0 Na-U | 8.16 | 2.09 | 3.26 | — | 9.80 | 0.53 | 22,000 | 604 | 27.5 | −0.61 |
| 1.0 Na-W | 8.23 | 1.42 | 9.15 | — | 5.58 | 0.90 | 25,000 | 583 | 24.3 | −0.14 |
| 5.0 Na-W | 7.95 | 0.86 | 11.66 | — | 13.70 | 0.89 | 36,000 | 714 | 19.8 | −0.68 |
| 0.05 Ca-W | 7.74 | 0.25 | — | 13.4 | 1.66 | 0.91 | 17,000 | 477 | 28.0 | |
| 0.5 HCl | 4.92 | — | 143.5 | 24.7 | 1.02 | 17.18 | 142,000 | 762 | 5.4 | |
| 1.0 NaOAc | 5.07 | — | 172.7 | 214.7 | 6.53 | 21.60 | 142,000 | 788 | 5.5 | |

(Negative value for $^T$Sr due to blank correction; *7 day values*; $^T$Sr rounded to appropriate precision.)

that had precipitated with calcium carbonate during the waste intrusion event, and $^T$Sr$^{2+}$ that had been co-precipitated with $Ca^{2+}$ in calcite that pre-existed waste release. There were therefore two solid-phase compartments for Sr that were not at global isotopic equilibrium: (i) pre-existing calcite and (ii) the exchanger phase plus secondary calcite. Calcite that was $^{90}$Sr-poor and present before the intrusion of waste solutions was dissolved by HCl and NaOAc and caused a decrease in the $^{90}$Sr/$^T$Sr through isotopic dilution.

### 3.3.2. Carbonate-component ions

The leachate components inorganic carbon, calcium, and pH showed progressive concentration relationships with changing extracting solutions, but the relationships were not in the same order for the three ions (Table 2). $HCO_3^-$ concentrations decreased with an increasing ionic strength of the extracting solutions (Fig. 4a). $Ca^{2+}$ concentrations, like $Sr^{2+}$ concentrations, increased with an increasing ionic strength of the extracting solutions (Fig. 4b). Also, for a given extracting solution, the amount of $Ca^{2+}$ released from washed sediment was larger than the amount released from unwashed sediment, and the inverse relationship applied to $HCO_3^-$. The pH varied systematically between extracting solutions; the pH in leachates of higher ionic strength was lower, with only slight differences in pH between washed and unwashed sediment (Fig. 4c and

Table 2). In a separate experiment (not shown), sediment was progressively washed while monitoring the release of $HCO_3^-$, yielding a total of approximately 7.4 μmol $HCO_3^-$ $g^{-1}$.

### 3.3.3. Potassium and magnesium

Mg is readily incorporated in the calcite mineral structure, but K is not.

The release of $K^+$ (Fig. 5a) increased in a sequence from lower to higher ionic strength of the extracting solution. Although the greatest concentration was obtained from washed sediment, and was significantly higher than from unwashed sediment, the relationship across extractants was not consistent with the results for other cations. The values for 0.5 mol $L^{-1}$ HCl were lower than those for 0.05 mol $L^{-1}$ $Ca^{2+}$, and the values for 1 mol $L^{-1}$ NaOAc and 1 mol $L^{-1}$ $NaNO_3$ were approximately equivalent. $Mg^{2+}$ (Fig. 5b) paralleled $Ca^{2+}$ (Fig. 4b) in its behavior, with the greatest leachate concentrations from 0.05 mol $L^{-1}$ HCl and 1 mol $L^{-1}$ NaOAc, and distinctly greater concentrations from washed compared to unwashed sediment.

### 3.3.4. Cation exchange capacity

The cation exchange capacity (CEC) was estimated from desorption data for 5 mol $L^{-1}$ $NaNO_3$ and 0.05 mol $L^{-1}$ $CaNO_3$, and from extraction with 1 mol $L^{-1}$ $NH_4Cl$ (Table 3). The data were consistent, indicating a CEC of 53 μeq $g^{-1}$ of sediment, with exchange sites dominated by $Na^+$, $K^+$, and $Ca^{2+}$. This CEC was low compared to typical soils in arid environments, e.g., 160 μeq $g^{-1}$ (Sposito, 1989), but consistent with the coarse nature of the H2 sediment. The CEC was not changed by the sediment washing process.

### 3.4. Autoradiography

For autoradiography, three samples collected within the zone of elevated $^{90}Sr$ above 21.5 m depth were examined, i.e., at 15.4, 16.2, and 18.5 m depth (Samples designated 20A, 21A, and 26A, respectively). Screening to determine whether $^{90}Sr$ was preferentially concentrated in clasts of restricted lithology or lithologies, using loose sediment disseminated on autoradiography plates, showed that non-radioactive clasts were generally monomineralic silicate minerals including quartz and feldspar. The radioactive particles were lithic fragments. Thin sections were evaluated for how well their total activity, measured by arbitrary but internally consistent photostimulated luminescence (PSL) units (Zeissler et al., 1998, 2001), compared with the liquid scintillation measurements of sediment leachates. PSL units correlated with residual activity calculated from leachate results (not shown), and the distribution of $^{90}Sr^{2+}$ on autoradiography images of thin sections was assumed to accurately represent its distribution in the sediments.

Consistent with loose-sediment screening, the autoradiography results for the thin sections showed that $^{90}Sr$ was highly enriched in selected clasts (Fig. 6), and concentrated in a relatively small fractional area of each of these clasts. In the figure, backscattered electron images (BSE) of the thin sections are overlain with transparent corresponding autoradiographs (AR). For presentation, both images are shown inverted: lighter areas on the autoradiograph represent more intense radioactivity, and darker areas on the thin section represent material with a higher average atomic number. Essentially all $^{90}Sr$ in these sediments was associated with basaltic lithic fragments. One area of $^{90}Sr$ concentration, indicated by an arrow in Fig. 6, is keyed to Fig. 7. For comparison, non-inverted BSE and AR of Sample 26 (Fig. 6: BSE and AR) clearly show the association of $^{90}Sr$ with basalt fragments, which comprise a significant fraction of the Hanford formation (Bjornstad, 1990). The BSE images illustrate the coarse, clay-deficient nature of these sediments; the smallest clasts were approximately 5–10 μm across.

The major contributor of lithic fragments to the Hanford formation was the underlying Columbia River Bas-

Table 3
Cation exchange capacity for Sample 26A estimated from different extraction conditions

|  | Extractant | | | |
|---|---|---|---|---|
|  | Unwashed[b] 1 mol $L^{-1}$ $NH_4Cl$ | Unwashed[a] 5 mol $L^{-1}$ $NaNO_3$ and 0.05 mol $L^{-1}$ $Ca(NO_3)_2$ | Unwashed[a] 1 mol $L^{-1}$ $NaNO_3$ and 0.05 mol $L^{-1}$ $Ca(NO_3)_2$ | Washed[a] 5 mol $L^{-1}$ $NaNO_3$ and 0.05 mol $L^{-1}$ $Ca(NO_3)_2$ |
| Total[c] ($\mu$eq $g^{-1}$) | 52.8 | 53.7 | 48.7 | 52.2 |
| E(Na)[d] | 0.343 | 0.676 | 0.745 | 0.256 |
| E(K) | 0.088 | 0.183 | 0.116 | 0.260 |
| E(Ca) | 0.569 | 0.121 | 0.115 | 0.447 |
| E(Mg) | ND | 0.020 | 0.023 | 0.034 |
| E($^T$Sr) | 0.00082[e] | 0.00082[e] | 0.00035 | 0.0014 |

[a] Fourteen day extraction.
[b] Two hour extraction with water followed by two hour extraction with $NH_4Cl$.
[c] Sum of extractable Na, K, Ca, Mg, and Sr.
[d] Fractional equivalents.
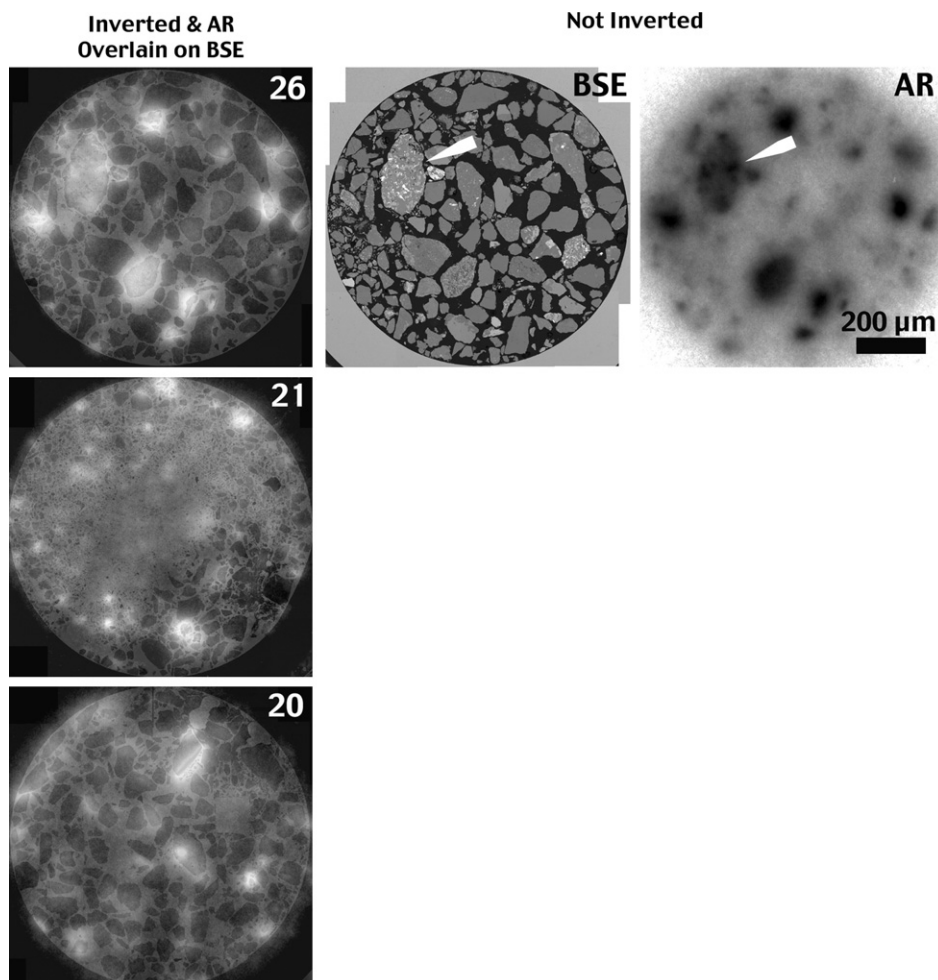[e] i.e., 0.022 mmol $kg^{-1}$.

Fig. 6. Backscattered electron images (BSE) and autoradiographs (AR) of Samples 20A, 21A, and 26A. Images inverted and transparent AR overlain on BSE for all samples, and non-inverted BSE and AR images for Sample 26A alone.
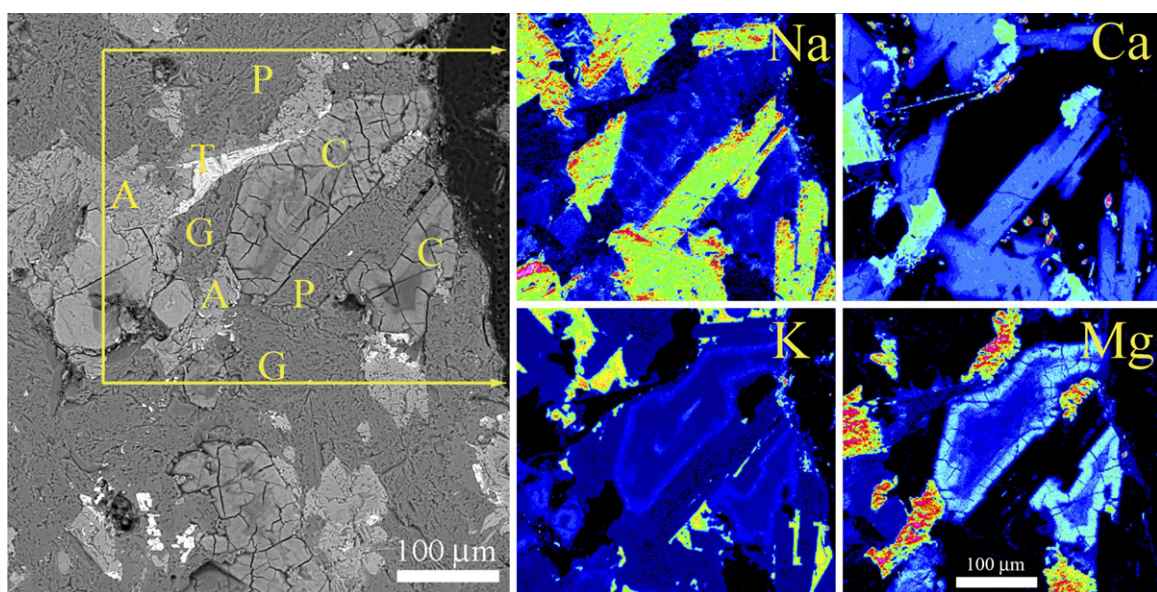


Fig. 7. BSE and elemental abundances for the area of smectite inclusions keyed by the arrow in Fig. 6. In false color, blue is least abundant and red most abundant in a rainbow progression; in black and white, white is most abundant. (For interpretation of color mentioned in this figure the reader is referred to the web version of the article.)

alts, which included primary phases that would not be expected to significantly adsorb $Sr^{2+}$. The basalts consisted of varying proportions of augite, plagioclase, titanomagnetite, and glass (Allen, 1985; Long and Wood, 1986). Collonade basalts (massive columnar outcrops) included compositionally homogeneous glass, and entablature basalts (massive non-columnar outcrops) included glass that separated into immiscible phases prior to solidification.

Detailed inspection of basalt fragments by SEM and EMP (Fig. 7), showed that glass weathered to form pockets of phyllosilicate clay (smectite) within these particles. The compositional abundance maps in Fig. 7 illustrated the relationship of smectite to primary basaltic phases. Na was distributed in plagioclase feldspar (laths) and unweathered glass (irregular morphology), and in the smectite inclusions (blue mottled areas). Ca was present also in plagioclase feldspar [$(Na,Ca)(Al,Si)AlSi_2O_8$] and glass, and in augite [$Ca(Mg,Fe,Al)(Al,Si)_2O_6$], and was absent as expected in the Na-saturated smectite. Mg was present most abundantly in augite, but Mg and K were differentially present within the smectite field, associated with compositional banding inherited apparently during precipitation. The smectite areas had replaced glassy mesostasis, and included dessication cracks. The banded clay was identical in appearance and qualitative composition to the smectite formed in weathered basalts, where it occurs as saponite or beidellite (McKinley et al., 1986). The mean composition of ten EMP analyses of 11 points at random within the smectite inclusions in Fig. 7 assuming eleven oxygen atoms, was $(Na,Ca,K)_{0.19}(Al,Mg,Fe)_{2.27}(Al,Si)_4O_{10}(OH)_2$, consistent with clay minerals within the montmorillonite group (Deer et al., 1976b).

# 4. Discussion

## 4.1. Extraction experiments

It was known from the inventory of tank wastes (Jones et al., 2001) that the tank waste solution that intruded into the vadose zone was alkaline, with relatively high concentrations of dissolved sodium and bicarbonate, and the composition and pH of pore waters from samples above a depth of 26 m reflected the contribution of the tank waste. Sediment 26A was washed repeatedly with deionized water to remove soluble carbonate and to quantify its potential effects, and experiments were conducted with washed and unwashed sediments. During experimentation, in all cases, the concentration of $HCO_3^-$ increased along with $Ca^{2+}$ over the course of the extraction experiments, indicating that calcite dissolved during extraction whether or not the sediment had been pre-washed. The hypothetical removal of bicarbonate solid or liquid phases did not significantly affect the results.

### 4.1.1. Two component reaction model

The experimental results and the texture of subsurface sediments led to the formulation of the conceptual model

represented in Fig. 2. The experiments were conducted on a sediment impacted by tank waste, in which $CaCO_3$ coexisted with an exchanger phase that was essentially saturated with $Na^+$. It was our hypothesis that the reactivity of the sediment could be described using the two-component, calcium carbonate-exchanger phase system. The response of the $Na^+$-saturated sediment during extraction with different solutions is represented schematically in the lower part of Fig. 2. All of our experimental results were consistent with this model.

During reaction with deionized water, calcite dissolved, and solution $Ca^{2+}$ was rapidly exchanged for $Na^+$, leaving a solution of $Na^+$ and $HCO_3^-$. When the sediment was extracted with 5 mol $L^{-1}$ $Na^+$, the extracting solution dissolved $CaCO_3$, but did not interact with the $Na^+$-saturated exchanger, and the solution included $Na^+$, $Ca^{2+}$ and $HCO_3^-$. When the sediment was extracted with 0.05 mol $L^{-1}$ $Ca^{2+}$, the solution dissolved $CaCO_3$ to release a small amount of $HCO_3^-$, and $Ca^{2+}$ equilibrated with the exchanger, releasing significant $Na^+$ and resulting in a solution that included $Ca^{2+}$, $Na^+$, and $HCO_3^-$.

In each extraction, the dissolution of calcite was dependent on the steady-state conditions necessary to reach or approach saturation. For extraction with deionized water, cation exchange removed $Ca^{2+}$ from solution, requiring greater dissolution of $CaCO_3$ to reach saturation; the amount of $CaCO_3$ dissolution was equivalent to the concentration of $HCO_3^-$. For extraction with 1 and 5 mol $L^{-1}$ $Na^+$, $Ca^{2+}$ was not as effectively removed from solution by the exchanger, less $CaCO_3$ was dissolved, and the concentration of $HCO_3^-$ was lower. Finally, for extraction with 0.05 mol $L^{-1}$ $Ca^{2+}$, only a small addition of $HCO_3^-$ was necessary to bring the solution phase near saturation with respect to $CaCO_3$, and little $CaCO_3$ was dissolved.

The relationship between the concentration of $HCO_3^-$ and $Ca^{2+}$ over the range of extractant solutions was due to the solubility relationship:

$$CaCO_3 = Ca^{2+} + CO_3^{2-} \qquad (1)$$

$$K_{sp} = [Ca^{2+}][CO_3^-]$$

The concentration of $Ca^{2+}$ was dramatically affected by reaction with the exchanger phase, and indirectly determined the steady state concentration of $HCO_3^-$. For each of the reaction paths represented in Fig. 2, the relevant $Ca^{2+}:Na^+$ and $Ca^{2+}:HCO_3^-$ were calculated and included on the figure. The values for the pristine system were from Sample 113 (Table 1), and the values for waste-impacted sediment were from Sample 38a (Table 1). The ratios for extractions of Sample 26A were derived from experimental data (Table 2) and, for extraction with deionized water, from the data as plotted in Fig. 1 (Serne et al., 2002a). Prior to waste intrusion, the molar ratios were within the range 0.4–1.4; after waste intrusion, the ratios were much less than 1; and the ratios after extraction with deionized water, 5 mol $L^{-1}$ $Na^+$, and 0.05 mol $L^{-1}$ $Ca^{2+}$ ranged from much

less than 1 to much greater than 1, all depending on the extent of calcite dissolution during extraction.

### 4.1.2. Dependence of pH

The $\log K_{sp}$ for reaction (1) at circumneutral pH and 25 °C is approximately $-8.5$. In natural environments, the effect of calcite dissolution on pH during the intrusion of groundwater solutions would be minor, because at circumneutral pH the product of the dissolving ions would rapidly bring the pore solution into equilibrium with respect to $CaCO_3$. In a field study where $CaCO_3$ dissolved and $Ca^{2+}$ was moderated by ion exchange (Zhu and Burden, 2001), pH was correlated with $Ca^{2+}$ and increased from 3.8 to 6.5, while $Ca^{2+}$ and $HCO_3^-$ increased by 8 and 23 mmol $L^{-1}$, respectively. For example, in our experiments, the pH was highest when the sediment was reacted with the extracting solution with the lowest ionic strength. In the experiments, the two-component reaction system (Fig. 2) where the exchanger was $Na^+$ saturated, would remove $Ca^{2+}$ from solution as $CaCO_3$ dissolved, driving the pH upward through the aqueous speciation reaction,

$$CO_3^{2-} + H^+ = HCO_3^- \qquad (2)$$

until the solubility relationship was satisfied. At higher ionic strengths and where $Ca^{2+}$ was used as an extractant, less dissolution would be required because the capacity for the exchanger to control the aqueous concentration of $Ca^{2+}$ would be limited by exchange with the extractant cation. The 1:1 relationship of $Ca^{2+}$ to $HCO_3^-$ can be seen readily in the timed extraction results using 5 mol $L^{-1}$ $Na^+$, where the sorption of $Ca^{2+}$ was inhibited (Fig. 8a). The dissolution of calcite was moderate within the overall results (2.09 µmol $g^{-1}$; Table 2), and the final pH was intermediate (8.16; Table 2). In the experiments overall (the fourteen-day extraction results for all extractants except HCl and NaOAc), the change in pH had a direct relationship to the extent of $CaCO_3$ dissolution represented by the concentration of $HCO_3^-$ (Fig. 8b). Because pH is an exponential function of the proton activity, the regression in Fig. 8b specifies that less than one net initial solution proton was complexed for each $CO_3^{2-}$ ion introduced into solution, and, except that the pH was a function of the dissolution of $CaCO_3$, the relationship was empirical. The two-component reaction assumption ignored other reactions, which could include proton desorption by cations in the electrolyte solution, deprotonation of amphoteric surface hydroxyl sites, desorption and hydrolysis of $Al^{3+}$ to liberate $H^+$, or dissolution reactions. At higher pH these relatively minor reactions could act to buffer the effects of carbonate dissolution on $[H^+]_{aq}$.

### 4.1.3. Strontium and the effects of sediment washing

As noted above, $^{90}Sr^{2+}$ and $^TSr^{2+}$ behaved chemically the same but were resident in two solid-phase pools, the exchanger and the total pool of $CaCO_3$, which were not in isotopic equilibrium with respect to Sr. The average of the HCl and NaOAc extracted $Ca^{2+}$ (158 µmol $g^{-1}$;
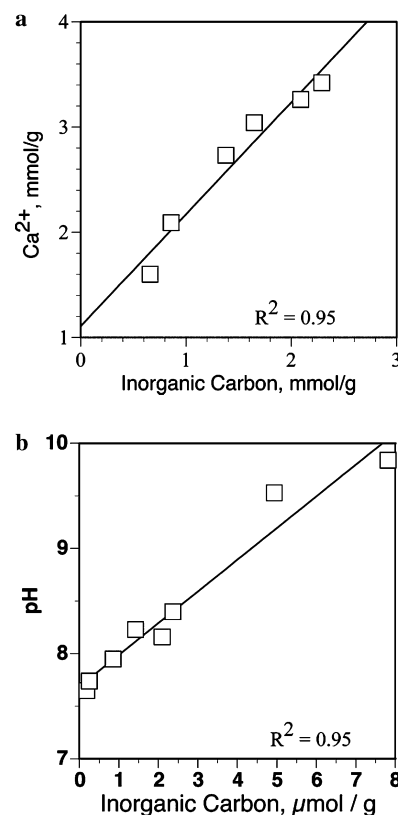
Fig. 8. (a) $Ca^{2+}$ as a function of $HCO_3^-$ for extraction with 5 mol $L^{-1}$ $Na^+$. (b) pH as a function of $HCO_3^-$ after 14 days of extraction for extraction with all solutions.

Table 2) was equivalent to dissolution of 15.6 mg carbonate $g^{-1}$, a calcium carbonate bulk concentration of approximately 1.6 wt%. The inorganic carbon concentration in the 5 mol $L^{-1}$ $NaNO_3$ extractions for washed and unwashed sediments (approximately 1 and 2 µmol $g^{-1}$, respectively) was equivalent to the dissolution of much less than 1% of the total calcite. The total $^{90}Sr^{2+}$ was approximately 0.775 pmol $g^{-1}$ (Table 2), and the extraction of $^{90}Sr^{2+}$ relative to $^TSr^{2+}$ (Fig. 9a) indicated that the cation extractions removed a maximum of approximately 80% of the $^{90}Sr^{2+}$ and 25% of the $^TSr^{2+}$ from the sediments. In contrast, the extraction by HCl and NaOAc, in which exchange and dissolution took place together, dissolved all of the available $CaCO_3$, and yielded the total of 140,000 pmol $^TSr^{2+}$ $g^{-1}$. The small amount of carbonate dissolved in the cation leachate solutions, 1–2 µmol $g^{-1}$ noted above, thus released a disproportionate fraction of the total $^{90}Sr^{2+}$. The extraction data for $^TSr^{2+}$ relative to $Ca^{2+}$ (Fig. 9b; results from $Na^+$ extractions, open and closed circles) indicated that the ratio of $^TSr^{2+}$ to $Ca^{2+}$ on the exchanger phase was much larger than the ratio in the pre-existing $CaCO_3$, since the data for $Na^+$ extraction had a much steeper slope. There were thus two pools of $^{90}Sr$ available for leaching ($^{90}Sr^{2+}$ on the smectite exchanger, and $^{90}Sr^{2+}$ coprecipitated with waste-induced calcite) and three pools of $^TSr$ ($^TSr^{2+}$ that was on the smectite exchanger,
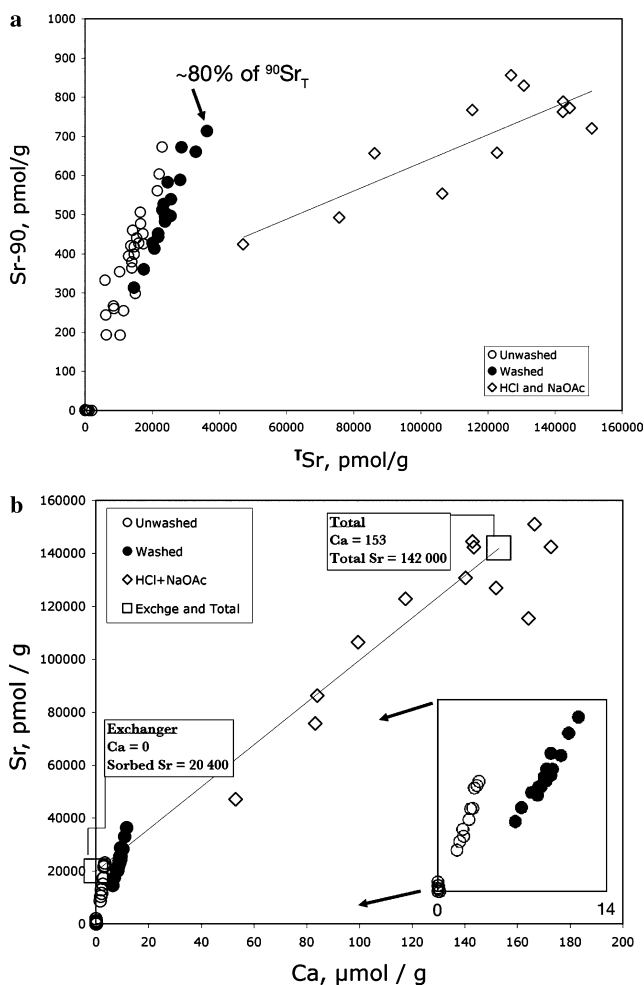
Fig. 9. (a) $^{90}Sr^{2+}$ as a function of $^{T}Sr^{2+}$ for all extractions. (b) $^{T}Sr^{2+}$ as a function of $Ca^{2+}$ for all extractions except $Ca^{2+}$. (Inset) detail of washed and unwashed cation extraction results.

that was coprecipitated with $^{90}Sr^{2+}$ in calcite, and that was coprecipitated in pre-existing calcite without included $^{90}Sr$).

The residence of $^{90}Sr$ in waste-induced $CaCO_3$ may have been influenced by rapid precipitation and the incorporation of significant $Mg^{2+}$ within it. $Mg^{2+}$ is readily incorporated as a substitution for $Ca^{2+}$ in the calcite structure. Numerous studies have shown that the calcite structure relaxes or contracts to accommodate such elemental substitutions (Cheng et al., 1998; Xu et al., 1996; Reeder et al., 1999). For $Sr^{2+}$, in particular, which has a slightly larger ionic radius than $Ca^{2+}$, the substitution is facilitated by the presence within the structure of $Mg^{2+}$, which has a smaller ionic radius than $Ca^{2+}$ (Mucci and Morse, 1983). The partition coefficient for $Sr^{2+}$ to calcite is also larger at higher precipitation rates (Tesoriero and Pankow, 1996; Rimstidt et al., 1998). The apparently high concentrations of $HCO_3^-$ within the waste solution and precipitation of $CaCO_3$ near the site of desorption within the basalt clasts may thus have facilitated the removal of $^{90}Sr^{2+}$ from solution.

The (14 day) total $Ca^{2+}$ and $^{T}Sr^{2+}$ results, and the results from 5 mol $L^{-1}$ $Na^+$ extraction could be used to estimate the amount of $^{T}Sr$ substituted in the pre-existing $CaCO_3$. The two results are plotted in Fig. 9b (large squares). Taking the differences between the two results and dividing by the total $Ca^{2+}$, the incorporation of Sr in $CaCO_3$ was approximately 784 pmol $^{T}Sr$ per μmol of $CaCO_3$.

The effect of sediment washing was shown by the relationship of $Na^+$ extraction data for the two sets of experiments (inset, Fig. 9b). Extraction after washing released more $^{T}Sr^{2+}$ and $Ca^{2+}$, and the proportion of $Ca^{2+}$ to $^{T}Sr^{2+}$ was greater. Because washing was equivalent to extraction with deionized water, it acted to dissolve $CaCO_3$, whose cationic components were exchanged for $Na^+$. The washed-sediment results thus conformed to the two-component reactive model for this sediment. The incorporation of $^{90}Sr$ into waste-induced $CaCO_3$ was also apparent through comparison of $Na^+$ extractions (1.0 and 5.0 mol $L^{-1}$) from washed and unwashed sediments (Table 2). The amount of $^{90}Sr^{2+}$ extracted from washed sediments was larger, but the ratio of $^{90}Sr^{2+}$ to $^{T}Sr^{2+}$ was smaller, indicating that the solid-phase pools of $^{90}Sr$-containing $CaCO_3$ were dissolved in different proportions; more total $CaCO_3$ was dissolved during washing and subsequent extraction, and the contribution of pre-existing, $^{90}Sr$-poor $CaCO_3$ was greater.

### 4.2. Autoradiography and reaction kinetics

Although cation exchange is a rapid process (Sposito, 1984), all of the desorbing ions required seven days or more to reach steady-state values (Figs. 3–5). The slow ion release was consistent with an exchanger phase located within basalt clasts of heterogeneous mineralogy (Figs. 6 and 7). Though the solid-solution exchange was rapid, the overall approach to equilibrium would be slowed by cationic diffusion to and from clast interiors into pore space. The spatial distribution of calcite containing $^{90}Sr$ was determined by the autoradiography results. Because all of the $^{90}Sr$ was associated with spatial regions of secondary smectite in basalt clasts (Fig. 6), the calcite with which $^{90}Sr^{2+}$ was coprecipitated must have precipitated on or near the smectite. The waste solutions included abundant $HCO_3^-$, so that $Ca^{2+}$ desorbed from the smectite phase by $Na^+$ may have caused calcite saturation and precipitation proximal to the smectite phase during waste infiltration. Pre-existing calcite is known to act as a template for $Sr^{2+}$ coprecipitation in secondary calcites (Astilleros et al., 2003), and this process may have contributed to the localization of $^{90}Sr$.

Autoradiography was used to investigate the diffusion and migration of $^{90}Sr^{2+}$ in granites as part of the investigation of nuclear waste in Sweden (Pinnioja et al., 1985; Suksi et al., 1986; Suksi et al., 1987; Ittner et al., 1988). Although the scale of those investigations was coarser than the scale of our observations, the results confirmed the role of secondary phases in sorbing and transmitting $^{90}Sr^{2+}$ in relatively non-

reactive lithologies. The fracture fill minerals—'micaceous and clayey material'—acted as sorbents and conduits through the rock matrix. Diffusivities for $^{90}Sr^{2+}$ in fractures occupied by secondary phases were $0.5–3.4 \times 10^{-14}$ m$^2$ s$^{-1}$, and $^{90}Sr^{2+}$ had penetrated granite cores along the fractures to a depth of 35 mm after one year of exposure.

### 4.3. Exchange modeling

The experimental results indicated that the evolution of ion concentrations in our experiments was explained by cation exchange of K$^+$, Ca$^{2+}$, Mg$^{2+}$, $^T$Sr$^{2+}$, and $^{90}$Sr$^{2+}$, on secondary smectite within weathered basalt clasts, and by the simultaneous dissolution of solid phases, particularly CaCO$_3$, which contributed Ca$^{2+}$, Mg$^{2+}$, $^T$Sr$^{2+}$, and $^{90}$Sr$^{2+}$ to solution. The interpretation of the results using an ion exchange model was thus complicated by the changing contribution of dissolution in experiments using different extracting solutions.

For modeling purposes, the total ion concentrations were estimated from the CEC and electrolyte extraction data (Tables 2 and 3). For all of the extraction experiments, the initial exchanger-resident concentration of the cations Na$^+$, K$^+$, Ca$^{2+}$, Mg$^{2+}$, $^T$Sr$^{2+}$, and $^{90}$Sr$^{2+}$ was assumed to be constant. The contribution due to dissolution of CaCO$_3$ for each of these cations was added to the sorbed concentration to derive total concentrations for evaluation by a cation exchange model for each extraction of unwashed sediment (Table 4). The specific derivations of the sorbed

and total concentrations are given in footnotes to Table 4, but some further clarification is required.

For K$^+$, the CEC value (Table 3) was used as the *exchanger* concentration. For the other cations, *exchanger* concentrations were derived from 5 mol L$^{-1}$ Na$^+$ extraction data. The values were corrected to include the contribution from calcite dissolution during extraction, as follows. The inorganic carbon concentration was taken to represent dissolved CaCO$_3$ (Fig. 8a), and the Ca$^{2+}$ concentration equivalent to the inorganic carbon concentration after extraction (2 μmol inorganic carbon g$^{-1}$ sediment$^{-1}$) was subtracted from the 5 mol L$^{-1}$ Na$^+$ extraction value for Ca$^{2+}$, and that Ca$^{2+}$ concentration was used as the *exchanger* concentration. The $^T$Sr contribution from calcite dissolution (784 pmol $^T$Sr μmol$^{-1}$ calcite$^{-1}$) was estimated from the Ca$^{2+}$–$^T$Sr$^{2+}$ relationship shown in Fig. 9b, and 1600 pmol g$^{-1}$ was subtracted from the extraction value for the 5 mol L$^{-1}$ Na$^+$ $^T$Sr$^{2+}$, and used as the *exchanger* concentration. The $^{90}$Sr$^{2+}$ contribution from calcite dissolution was more difficult to assess, because there were two pools of Sr-bearing calcite. The contribution from dissolution of $^{90}$Sr-bearing calcite was estimated from the difference in results for the 5 mol L$^{-1}$Na$^+$ extraction of washed and unwashed sediments (Table 2). The difference in Ca$^{2+}$ concentration between washed and unwashed sediments was 8.4 μmol g$^{-1}$, and the difference in $^{90}$Sr$^{2+}$ concentration was 110 fmol g$^{-1}$, so the contribution from calcite dissolution was approximately 13 fmol $^{90}$Sr$^{2+}$ μmol$^{-1}$ calcite$^{-1}$, and the $^{90}$Sr$^{2+}$ equivalent to 2 μmol

Table 4
Input conditions for modeling and modeled equilibrium concentrations

| Leachant Exchanger: | IC[a] (μmol g$^{-1}$) | Na[b] (μmol g$^{-1}$) 43 | Ca (μmol g$^{-1}$) 1.17[c] | K (μmol g$^{-1}$) 4.66[d] | Mg (μmol g$^{-1}$) 0.53[a] | $^T$Sr (pmol g$^{-1}$) 20,400[c] | $^{90}$Sr (fmol g$^{-1}$) 578 | pH |
|---|---|---|---|---|---|---|---|---|
| | *Total initial concentration* | | | | | | | |
| DIW | 7.81 | 43 | 8.98[e] | 20.26 | 0.84 | 26523 | 775[f] | 9.84 |
| 0.01 Na | 4.93 | 63 | 6.10[e] | 14.50 | 0.73 | 24,265 | 775[f] | 9.53 |
| 0.05 Ca | 0.19 | 43 | 101.36[e] | 5.02 | 0.54 | 20,548 | 580 | 7.65 |
| 1.0 Na | 2.37 | 2043 | 3.54[e] | 9.38 | 0.62 | 22,258 | 608 | 8.40 |
| 5.0 Na | 2.09 | 10,043 | 3.26[e] | 8.82 | 0.61 | 22,038 | 604 | 8.16 |
| | *Modeled equilibrium aqueous concentration* | | | | | | | |
| DIW | 7.81 | 29 | 0.05 | 1.75 | 0.01 | 99 | 0 | 9.84 |
| 0.01 Na | 4.93 | 38 | 0.02 | 0.97 | 0.00 | 48 | 0 | 9.53 |
| 0.05 Ca | 0.19 | 43 | | 3.50 | 0.46 | 15000 | 462 | 7.65 |
| 1.0 Na | 2.37 | 1998 | 2.81 | 6.15 | 0.49 | 17583 | 458 | 8.40 |
| 5.0 Na | 2.09 | 9994 | 3.25 | 7.66 | 0.56 | 22038 | 604 | 8.16 |

'*Exchanger*' concentrations were the estimated exchanger-resident concentrations in the sediment prior to contact with extractant solutions. *Total initial concentrations*: used to initiate exchange modeling, equal to dissolved cations plus cations on the exchanger and cations dissolved from calcite during extraction. *Modeled equilibrium aqueous concentrations*: the initial concentrations less cations removed by equilibration with the exchanger.

[a] Table 2.
[b] The CEC was fixed at 53 μeq g$^{-1}$ (Table 2), and Na$^+$ was set to the difference between that value and the sum of the other cation equivalents, i.e., 43 μmol g$^{-1}$. Experimental additions (e.g., 0.01 mol L$^{-1}$ Na, where the solid:solution was 1:2) were summed with this value.
[c] Sorbed Ca and $^T$Sr were derived from 5 M L$^{-1}$ NaNO$_3$ extraction data (Table 2; Fig. 3) after subtraction of the contribution from dissolution of 2.09 μmol g$^{-1}$ calcite.
[d] Sorbed K was set at the value after exchange with 1 mol L$^{-1}$ NH$_4$Cl (Table 3).
[e] Total Ca was set equal to the sorbed concentration plus the inorganic carbon concentration (Table 2), based on equimolar calcium and inorganic carbon contributions from calcite dissolution.
[f] Total $^{90}$Sr for extractions that dissolved 4.9 and 7.8 μmol g$^{-1}$ of calcite were set equal to the total $^{90}$Sr, as the average of HCl and NaOAc extractions (Table 2).

$CaCO_3$ g$^{-1}$ sediment$^{-1}$ (i.e., 26 fmol $^{90}Sr^{2+}$ g$^{-1}$) was subtracted from the 5 mol L$^{-1}$ Na$^+$ extraction result, and used as the *exchanger* concentration.

Estimates of the *total* ion concentrations used in modeling were made using the same logic used for estimating the sorbed concentrations. Results for extraction with deionized water, 0.01 mol L$^{-1}$ Na$^+$, 0.05 mol L$^{-1}$ Ca$^{2+}$, 1 mol L$^{-1}$ Na$^+$, and 5 mol L$^{-1}$ Na$^+$ from unwashed sediment were estimated and modeled. The difference in Mg$^{2+}$ concentrations between washed and unwashed sediment extractions using 5 mol L$^{-1}$ Na$^+$ allowed the estimation of Mg in calcite of approximately 4 mol %. That estimate was within the range of Mg substitution found in natural calcites (Deer et al., 1976a). In each model case, 4% of the leachate HCO$_3$ concentration was added to the sorbed Mg$^{2+}$ concentration to yield an estimate for *total* Mg$^{2+}$. Ca$^{2+}$, $^{90}Sr^{2+}$, and $^TSr^{2+}$ were treated similarly. The *total* concentration of K$^+$ was estimated empirically. After preliminary modeling, the calculated total K$^+$ was noted to increase at approximately twice the amount of inorganic carbon, so K$^+$ was added to the *total* at that ratio to inorganic carbon. The regional basalts were low in potassium, 1 wt% or less K$_2$O (Hyndman, 1972). Potassium may have been heterogeneously distributed in a readily weathered phase (such as mesostasis glass) which could indirectly contribute K$^+$. Other potential contributors, including potassium feldspar and granitic clasts, were present in the sediment also. The significance of the relationship between K$^+$ and inorganic carbon was unknown, and was intended to provide a reasonable total cation composition for modeling.

The resultant set of *total* cation concentrations was used in cation exchange modeling (Table 4). The estimated *total* concentration of $^TSr^{2+}$ and $^{90}Sr^{2+}$ varied within the set by about 25%, and *total* Ca$^{2+}$ increased by a factor of eight between the initial conditions and what was estimated after equilibration with deionized water.

We applied an ion exchange model (Lichtner and Zachara, 2005) developed by experimentation and the fitting of exchange constants, using similar, but uncontaminated, H2 sediments (Knepp, 2002) for Sr$^{2+}$, Ca$^{2+}$, Mg$^{2+}$, and Na$^+$. The ion exchange model was developed from binary and ternary electrolyte experiments (with Na$^+$, Ca$^{2+}$, Sr$^{2+}$, and Mg$^{2+}$), where the aqueous and exchanger compositions were determined at equilibrium. The geochemical modeling used the MINTEQA2 code (Allison et al., 1991), and included binary reactions to describe sodium exchange with calcium, magnesium, potassium, and strontium (Table 5), according to the relationship:

$$uBX_v + vA^{u+} = vAX_u + uB^{v+} \quad (3)$$

where $A$ and $B$ were exchanging chemical species, $X$ was the exchanger phase, and charge balance was maintained through the charge and stiochiometric constants $u$ and $v$. The equilibrium constant was then:

Table 5
Exchange reactions, aqueous species, reaction constants used in exchange modeling

|  |  | $K_g$ | log $K_r$ |
|---|---|---|---|
| *Exchange reactions* |  |  |  |
| 2NaX + Sr$^{2+}$ = SrX$_2$ + 2Na$^+$ |  | 90.402 | 3.218 |
| 2NaX + Ca$^{2+}$ = CaX$_2$ + 2Na$^+$ |  | 76.720 | 3.147 |
| 2NaX + Mg$^{2+}$ = MgX$_2$ + 2Na$^+$ |  | 36.869 | 2.829 |
| NaX + K$^+$ = KX + Na$^+$ |  | 21.010 | 1.322 |

| Species | Reaction | log $K$ | Source |
|---|---|---|---|
| *Aqueous species and their stability constants* |  |  |  |
| SrOH$^+$ | Sr$^{2+}$ + H$_2$O − H$^+$ = SrOH$^+$ | −13.177 | NIST |
| SrCO$_3$(aq) | Sr$^{2+}$ + CO$_3^{2-}$ = SrCO$_3$(aq) | 2.81 | NIST |
| SrHCO$_3^+$ | Sr$^{2+}$ + CO$_3^{2-}$ + H$^+$ = SrHCO$_3^+$ | 11.539 | NIST |
| SrNO$_3^+$ | Sr$^{2+}$ + NO$_3^-$ = SrNO$_3^+$ | 0.6 | NIST |
| NaNO$_3$ | Na$^+$ + NO$_3^-$ = NaNO$_3$ | −1.044 | GMIN |
| NaCO$_3^-$ | Na$^+$ + CO$_3^{2-}$ = NaCO$_3^-$ | 1.27 | NIST |
| NaHCO$_3$ | Na$^+$ + CO$_3^{2-}$ + H$^+$ = NaHCO$_3$(aq) | 10.079 | NIST |
| CaOH$^+$ | Ca$^{2+}$ + H$_2$O − H$^+$ = CaOH$^+$ | −12.697 | NIST |
| CaCO$_3$(aq) | Ca$^{2+}$ + CO$_3^{2-}$ = CaCO$_3$(aq) | 3.20 | NIST |
| CaHCO$_3^+$ | Ca$^{2+}$ + CO$_3^{2-}$ + H$^+$ = CaHCO$_3^+$ | 11.599 | NIST |
| MgOH$^+$ | Mg$^{2+}$ + H$_2$O − H$^+$ = MgOH$^+$ | −11.397 | NIST |
| MgCO$_3$(aq) | Mg$^{2+}$ + CO$_3^{2-}$ = MgCO$_3$(aq) | 2.92 | NIST |
| MgHCO$_3^+$ | Mg$^{2+}$ + CO$_3^{2-}$ + H$^+$ = MgHCO$_3^+$ | 11.339 | NIST |
| Calcite | Ca$^{2+}$ + CO$_3^{2-}$ = CaCO$_3$ | 8.48 | NIST |

$$K_g = \frac{\{B^{v+}\}^u}{\{A^{u+}\}^v} \frac{[AX_u]^v}{[BX_v]^u} = \frac{\{B^{v+}\}^u}{\{A^{u+}\}^v} \frac{[un_{AX_u}]^v}{[vn_{BX_v}]^u}[r_s\text{CEC}]^{u-v} \quad (4)$$

where $n$ was the number of sites occupied by each species, $r_s$ was the ratio of solid to liquid (kg L$^{-1}$), and CEC was the cation exchange capacity (meq kg$^{-1}$). For MINTEQ, the reaction constants ($K_r$, used computationally) were calculated from $K_g$ as follows (Table 5):

$$K_g = K_r\left(\frac{u^v}{v^u}[r_s\text{CEC}]^{u-v}\right) \quad (5)$$

The model included non-sorbing aqueous hydroxide, nitrate, and carbonate complexes of the four cationic components (Table 5), and calcite was allowed to precipitate under saturated conditions. The Davies convention was used to estimate activity coefficients. The Davies equation is not strictly valid for the solution at an ionic strength of 5 mol L$^{-1}$ (Stumm and Morgan, 1996), and the calculations reported for this electrolyte were assumed to be imprecise. However, the Pitzer model, which is valid to high ionic strength (above 5 mol L$^{-1}$) appropriately parameterized, was preliminarily applied to the 5 mol L$^{-1}$ starting compositions (not shown) with results similar to the MINTEQ results; the Davies equation and MINTEQ were used throughout for the sake of uniformity. The equilibrium pH was fixed for the calculations at the measured 14-day value (Table 2), and equilibrium constants for the exchange reactions were those previously fitted (Lichtner and Zachara, 2005; Knepp, 2002). The modeling represented a prediction of the data: no parameters were adjusted to maximize the model fit to the data. The calculation was an

equilibrium one and no attempt was made to describe either the rapid kinetic phase of desorption that occurred in the experiments between 0 and 5 days or the slow kinetic evolution of the system that occurred in some experiments, i.e., the modeling was an attempt to simulate steady-state aqueous concentrations that were achieved after 7 days of desorption.

As expected, the modeling calculated that calcite was undersaturated throughout the set of extraction experiments (i.e., calcite was dissolving). The model matched the measured $^TSr$ values well (Fig. 3a), except for the values for extraction with 0.05 mol $L^{-1}$ $Ca^{2+}$, which was underpredicted by about 6%. The measured values for $Ca^{2+}$ were also well matched by the model (Fig. 4b), indicating that the estimation of total $Ca^{2+}$ concentrations using inorganic carbon as a proxy (Fig. 8a) was accurate.

The simulations for $Mg^{2+}$ and $K^+$ were less successful. $Mg^{2+}$ (Fig. 5) was generally underpredicted. For extraction with $Na^+$, the agreement was within 15% of the measured value, but for extraction with $Ca^{2+}$ the disagreement was 35%. Also, the model predicted that $Ca^{2+}$ would extract less $Mg^{2+}$ than would $Na^+$, but the reverse was true. There was apparently an error made in evaluating one of the independent variables that went into the simulation, which included the exchange constant derived from isotherms (Lichtner and Zachara, 2005) and the estimates of the mole fraction of $Mg^{2+}$ in calcite and the surface resident $Mg^{2+}$ prior to extraction. The maximum difference between measured and modeled $Mg^{2+}$ concentrations was relatively small (0.24 μmol $g^{-1}$), however, and the modeling error relative to the overall CEC (53 μeq $g^{-1}$) would not be expected to affect simulations of $^{90}Sr^{2+}$ equilibrium. The modeling results for $K^+$ were also in disagreement with measured values (Fig. 5), but $K^+$ often shows complex ion exchange behavior and deviations were expected. The simulation was in the same order as the measured values, with $Ca^{2+}$ extraction predicted to remove less $K^+$ than $Na^+$ extraction. For extraction with 1 mol $L^{-1}$ $Na^+$, 5 mol $L^{-1}$ $Na^+$, and 0.05 mol $L^{-1}$ $Ca^{2+}$, the difference between measured and calculated $K^+$ values was 22–31%. The estimated total $K^+$ concentrations were also a significant fraction of the CEC (Table 3). The effects on the calculated sorption of $^TSr$, however, were likely to be minor. The $K_r$ for $K^+$ (Table 5) was one one-hundredth the $K_r$ for $^{90}Sr^{2+}$.

The model was used indirectly to evaluate whether cation exchange could explain the distribution of $^{90}Sr^{2+}$ in the extraction experiments. The behavior of $^{90}Sr^{2+}$ was expected to be identical to the behavior of $^TSr$. As described above, the total concentration of $^{90}Sr^{2+}$ for each extraction was calculated as the ion-exchangeable concentration (578 pmol $g^{-1}$) plus the contribution from calcite dissolution (13 pmol $^{90}Sr^{2+}$ μmol$^{-1}$ calcite$^{-1}$). The calcite contribution was calculated from the difference between washed and unwashed sediment extracted with 5 mol $L^{-1}$ $Na^+$, which represented the dissolution of 8 μmol calcite $g^{-1}$ sediment$^{-1}$. For extraction with deionized water and

0.01 mol $L^{-1}$ $Na^+$, all of the $^TSr$ was retained by the sediment (Table 2), and the respective model predictions were that negligible $^{90}Sr^{2+}$ would be extracted (Fig. 3). For extraction with 0.05 mol $L^{-1}$ $Ca^{2+}$, 1 mol $L^{-1}$ $Na^+$, and 5 mol $L^{-1}$ $Na^+$, the desorbed fractions were predicted to be 0.73, 0.79, and 1.00. Our methodology fixed the model in agreement with the extraction value at 5 mol $L^{-1}$ $Na^+$ based on previously performed laboratory experiments (Fig. 3). The model agreed with measured values to within 5% for 1 mol $L^{-1}$ $Na^+$ (predicting 458 pmol $g^{-1}$) and within 9% for 0.05 mol $L^{-1}$ $Ca^{2+}$ (predicting 462 pmol $g^{-1}$). The slight deviations between model and experiment were probably a consequence of our method for estimating the release of $^{90}Sr^{2+}$ from calcite. It was likely that the $^{90}Sr$ concentration in waste-precipitated calcite was higher than we estimated, and that the proportions of released $^{90}Sr^{2+}$ and $^TSr^{2+}$ changed rapidly during initial calcite dissolution. The dissolved $^{90}Sr^{2+}$ contribution from dissolution of 0.19 μmol calcite $g^{-1}$ during extraction with 0.05 mol $L^{-1}$ $Ca^{2+}$ would therefore be underestimated, and the dissolved $^{90}Sr^{2+}$ contribution from dissolution of 2.09 μmol calcite during extraction with 5 mol $L^{-1}$ $Na^+$ would be overestimated.

The predicted concentrations of $^{90}Sr^{2+}$ (Fig. 3b), the focus of this work, were remarkably close to the observed values. The accuracy of these predictions reinforces the generality of the cation exchange model that was developed elsewhere (Lichtner and Zachara, 2005). The kinetic behavior of the sediments during desorption may be explained by the partial physical isolation of the exchanger phase from the electrolyte solution. The five-day 'rapid' approach to steady state was slow for typical cation exchange. After the initial exposure to $^{90}Sr^{2+}$, the sub-tank sediments had at least thirty years to reach equilibrium and the $^{90}Sr^{2+}$ could thoroughly penetrate the smectite inclusions. Although our experiments used sediment suspensions with high dissolved cation concentrations relative to the solid-resident $^{90}Sr^{2+}$, the time scale of those experiments was apparently insufficient to reach more than approximate equilibrium with the physically sequestered intragrain smectite exchanger.

### 4.4. Borehole samples

Results from the chemical characterization of the borehole samples indicated that the wastes, with high concentrations of $Na^+$ and $HCO_3^-$, impacted pore water chemistry to a depth of about 50 m (Fig. 1). With respect to the displaced indigenous divalent cations, $Sr^{2+}$ and $Ca^{2+}$, though, the maximum impact was within the interval beginning a meter or two below the tank-farm backfill and extending to a depth of 25 m, where the water extractable concentrations of these cations were diminished by more than one order of magnitude. The base of the zone coincided with a thin confining bed.

Although vadose-zone contaminants at B-110 were attributed to a single transfer-line leak in the 1960s or

1970s, lateral movement of wastes at the B tank farm was noted (Knepp, 2002), and the most-leached interval could represent the lateral spreading of migrating tank wastes above the fine-grained interval of less transmissive sediment at a depth of 26 m (Fig. 1). Sediments within this interval may also have been repeatedly extracted by solutions from leaks that occurred from the broader area of the B Tank Farm (Corbin et al., 2001), or from earlier leaks of $Na^+$ bearing wastes from B-110. The timing of sodium bicarbonate waste infiltration is an important detail that affects the observation of $^{90}Sr^{2+}$ centered within the interval of lowest leachable $Ca^{2+}$ and $Sr^{2+}$. The occurrence of a lobe of acid-extractable $^{90}Sr^{2+}$ within the interval containing little or no water-leachable cations other than $Na^+$ (Fig. 1) was consistent with the introduction of $^{90}Sr^{2+}$ after cation exchange by sodium-bearing solutions from previous leaks, but was not consistent with deposition coincident with the displacement of indigenous $Sr^{2+}$. The precise history of operations at the B Tank Farm and the origin the individual waste components in the vadose zone beneath it are not known (Corbin et al., 2001; Knepp, 2002), and the simplest explanation for the removal of indigenous $Sr^{2+}$ and $Ca^{2+}$ and the implacement of $^{90}Sr^{2+}$ in these sediments is that they resulted from separate events. This conclusion is speculative, and the tank farm history and sequence of cation displacement and $^{90}Sr^{2+}$ emplacement do not affect the interpretations of our experimental results, or their implications for $^{90}Sr^{2+}$ mobility in the Hanford sediments.

The 1:1 extractions were intended to provide estimates of pore water compositions by extrapolation of the analytical results to concentration values for the original samples based on gravimetric water contents. Although the moisture contents varied, they were typically 4–5 wt%, requiring the application of a dilution correction to leachate compositions of approximately 25 (i.e., the compositions measured from leachates were multiplied by 25). The results of this procedure were at odds with the results from centrifugation (Table 1); the 1:1 water extraction results in Fig. 1, presented as ions extracted per gram of sediment, did not represent pore water compositions, because they resulted from pore water dilution, calcite and silicate mineral dissolution, and cation exchange during extraction; these reactions changed the pH and estimated composition of the porewater. However, the extraction values provided an accurate representation of the relative impact of waste solutions on the in situ sediment.

How could the two-component model be used to understand the relative impact of tank waste on vadose sediments, and provide information about the future behavior of solutions in the impacted sediment? The two-component reactivity model included interactions between cation exchange and carbonate dissolution during cation extraction experiments. Solution equilibrium with respect to the carbonate phase was moderated by cation exchange, which affected the solution concentration of cation carbonate com-

ponents, particularly $Ca^{2+}$. To approach equilibrium, the IAP for the carbonate phase was biased toward the inorganic carbon component, and aqueous equilibrium speciation reactions consumed $H^+$ to raise pH. The inorganic carbon and $H^+$ components were thus linked through the extent of $Na^+$ saturation on the exchanger phase. The two-component model was therefore applied to the water extraction results for the vadose zone by examining the relationship between extracted $HCO_3^-$ and pH. The results were similar to those for Sample 26A (Fig. 8b), except that pH varied empirically with inorganic carbon according to two independent relationships (Fig. 10). The first, labeled 'Series 1', was $pH = 0.48HCO_3^- + 7.08$ and had $R^2 = 0.89$, and the second ('Series 2') was $pH = 0.86HCO_3^- + 7.16$ and had $R^2 = 0.59$. When plotted onto the stratigraphic variation in pH (Fig. 10), the first series described the variation in pH of the 1:1 extractions for most of the stratigraphic interval, including the zone impacted most directly by waste intrusion, and the second series described the extractate pH for an intermediate interval that lay just below the waste-impacted zone. Other characterization data for the vadose sediments (not shown) indicated that the intermediate interval (Series 2) had acid extractable $Si^{4+}$ concentrations that were significantly higher than the surrounding sediments, and a higher total $SiO_2$ concentration as well (Serne et al., 2002a,b). It is plausible that the interval represented by 'Series 2' included solid phases with less buffering
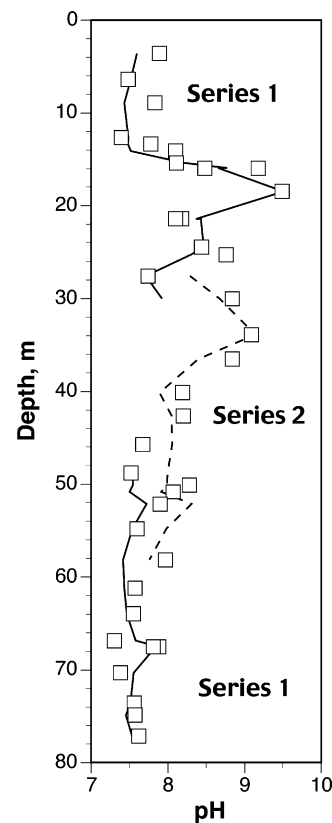


Fig. 10. 1:1 extraction pH compared to pH calculated from inorganic carbon concentrations separated into two intervals.

capacity, accounting for the steeper relationship and poorer correlation between pH and $HCO_3^-$. The overall relationship of $HCO_3^-$ with pH for sediments from the stratigraphic column down to the water table supports the validity of the two-component reactivity model and its application to the vadose sediments generally; cation exchange influenced the extent of carbonate dissolution and its impact upon solution pH.

## 5. Conclusion

A two-component model including an exchanger phase and $CaCO_{3(s)}$ to explain solution interaction with Hanford's waste-impacted sediments was tested using a representative sediment containing $^{90}Sr^{2+}$. The model replicated results from a range of $Na^+$ and $Ca^{2+}$ extraction solutions. Its extension to a broader set of core samples that represented the vadose strata at the site, through empirical estimations of the effect of calcite dissolution on pH, suggested that cation exchange and $CaCO_3$ solubility could control $^{90}Sr^{2+}$ mobility in the vadose zone, and that the model could aid in predicting $^{90}Sr^{2+}$ movement under likely geochemical scenarios. These field results have an experimental analogue. A simulation and modeling study by others (Condom et al., 2002) of a vadose environment including alkaline soils found that the migrating concentrations of $Ca^{2+}$, $Mg^{2+}$, $Na^+$, and $Cl^-$ could be described by cation exchange and dissolution of $CaCO_3$ and silicate minerals. Also, the use of the $Na^+$ saturation of cation exchange sites in soils through the addition of NaOH or $NaHCO_3$, followed by the subsequent precipitation of $CaCO_3$ through the addition of $CaCl_2$ to precipitate $^{90}Sr^{2+}$, was shown to be a feasible immobilization strategy in earlier experimental studies using soils from Oak Ridge, Tennessee (Spalding, 1980, 1981). This same reaction sequence occurred in situ at the Hanford site as a result of waste-sediment reaction in mildly calcareous subsurface sediments.

Our results indicate that the future mobility and migration of $^{90}Sr^{2+}$ beneath the Hanford site B Tank Farm can be predicted from likely compositions of the intruding aqueous phase. They also suggest that, under realistic environmental conditions, the movement of $^{90}Sr^{2+}$ would be very limited. The contaminant is sorbed to intra-grain smectite that is not easily accessible to migrating fluids. At present it is confined to shallow depths relative to the water table. Although the sorption of $^{90}Sr^{2+}$ was limited by exchange with $Na^+$ and with other cations including $Sr^{2+}$, its original migration was limited (Fig. 1), and the unsaturated sediment column beneath it is a large buffer against groundwater contamination.

## Acknowledgments

## References

Adams, S., Titus, R., Pietersen, K., Tredoux, G., Harris, C., 2001. Hydrochemical characteristics of aquifers near Sutherland in the Western Karoo, South Africa. *J. Hydrol.* **241**, 91–103.

Ahmad, S.H.S.S., 1995. Competitive adsorption of $^{90}Sr$ on soil sediments, pure clay phases, and feldspar minerals. *Appl. Radiat. Isot.* **46**, 287–292.

Ali, M.Y., 1995. Carbonate cement stratigraphy and timing of diagenesis in a Miocene mixed carbonate-clastic sequence, offshore Sabah, Malaysia: constraints from cathodoluminescence, geochemistry, and isotopic studies. *Sediment. Geol.* **99**, 191–214.

Allen, C.C., 1985. Characterization of reference Umtanum and Cohassett basalt, Sd-BWI-DP-053. Rockwell Hanford Operations, Inc., pp. 47.

Allison, J.D., Brown, D.S., Novo-Gradac, K.J., 1991. MINTEQA2/PRODEFA2, a geochemical assessment model for environmental systems: version 3.0 user's guide, US EPA, pp. 106.

Astilleros, J.M., Pena, C.M., Fernandez-Diaz, L., Putnis, A., 2003. Metastable phenomena on calcite {10–14} surfaces growing from $Sr^{2+}$–$Ca^{2+}$–$CO_3^{2-}$ aqueous solutions. *Chem. Geol.* **193**, 93–107.

ASTM, 1998. Test Method for Laboratory Determination of Water (Moisture) Content of Soil and Rock. American Society for Testing and Materials, pp. 25.

Bjornstad, B.N., 1990. *Geohydrology of the 218-W-5 Burial Ground, 200-West Area, Hanford Site, PNL-7336*. Pacific Northwest Laboratory, pp. 25.

Casey, W.H., Chai, L., Navrotski, A., Rock, P.A., 1996. Thermochemistry of mixing strontianite [$Sr(CO_3)(s)$] and aragonite [$CaCO_3(s)$] to form $Ca_xSr_{1-x}CO_3(s)$ solid solutions. *Geochim. Cosmochim. Acta* **60**, 933–940.

Cheng, L., Sturchio, N.C., Woicik, J.C., Kemner, K.M., Lyman, P.F., Bedzyk, M.J., 1998. High-resolution structural study of zinc ion incorporation at the calcite cleavage surface. *Surf. Sci.* **415**, L976–L982.

Chitra, S., Sasidhar, P., Lal, K.B., Ahmed, J., 1999. The effect of common alkali and alkaline earth metal cation to the sorption of strontium and cesium onto soil. *J. Ind. Pollut. Control* **15**, 65–72.

Conca, J.L., Wright, J.V., 1998. The UFA method for rapid, direct measurement of saturated and unsaturated soil transport properties. *Aust. J. Soil Res.* **36**, 291–315.

Condom, N., LaFolie, F., Hammecker, C., Maeght, J.-L., Marlet, S., 2002. Solute transport and geochemistry modeling in the vadose zone: application to soil salinization, alkalinisation, and sodification, Paper no. 1342. In: *Proceedings, 17th World Conference on Soil Science*, pp. 1342-1–1342-5.

Corbin, R.A., Jones, T.E., Simpson, B.C., Wood, M.I., 2001. *Preliminary Inventory Estimates for Single-Shell Tank Leaks in B, BX, and BY Tank Farms, RPP-7389*. CH2M Hill Hanford Group, pp. 50.

Deer, W.A., Howie, R.A., Zussman, J., 1976a. Rock-Forming Minerals, vol. 5. Non-Silicates. John Wiley, London.

Deer, W.A., Howie, R.A., Zussman, J., 1976b. Rock-Forming Minerals, vol. 3. Sheet Silicates. Longmans, London.

DeSimone, L.A., Howes, B.L., Barlow, P.M., 1997. Mass balance analysis of reactive transport and cation exchange in a plume of wastewater-contaminated groundwater. *J. Hydrol.* **203**, 228–249.

EPA, 1984. Test Method for the Determination of Inorganic Anions in Water by Ion Chromatography, Method 300.0A, EPA-600/4-84-017. U.S. Environmental Protection Agency.

EPA, 2000a. Inductively Coupled Plasma-Atomic Emission Spectrometry, Method 6010B. In EPA Publication SW-846, Test Methods for Evaluating Solid Waste, Physical/Chemical Methods, <http://www.e-pa.gov/epaoswer/hazwaste/test/sw846.htm/>. U.S. Environmental Protection Agency.

EPA, 2000b. Inductively Coupled Plasma-Mass Spectometry, Method 6020. In Publication SW-846, Test Methods for Evaluating Solid Waste, Physical/Chemical Methods, <http://www.epa.gov/epaoswer/haswaste/test/sw846.htm/>. U.S. Environmental Protection Agency.

Hyndman, D.W., 1972. Petrology of Igneous and Metamorphic Rocks. McGraw-Hill, New york.

Ittner, T., Torstenfelt, B., Allard, B., 1988. Migration of the fission products strontium, technetium, iodine, cesium and the actinides neptunium, plutonium, americium in granitic rock. SKB, pp. 56.

Jones, T.E., Simpson, B.C., Wood, M.I., Corbin, R.A., 2001. Preliminary Inventory Estimates for Single-Shell Tank Leaks in B, BX, and BY Tank Farms, RPP-7389. CH2MHill Hanford Group, pp. 26.

Knepp, A.J., 2002. Field Investigation Report for Waste Management Area B-BX-BY, RPP-10098. U.S. Department of Energy, pp. 100.

Langmuir, D., 1971. The geochemistry of some carbonate ground waters in central Pennsylvania. *Geochim. Cosmochim. Acta* **35**, 1023–1045.

Lefevre, F., Sardin, M., Schweich, D., 1993. Migration of strontium in clayey and calcareous sandy soil: precipitation and ion exchange. *J. Contam. Hydrol.* **13**, 215–229.

Lefevre, F., Sardin, M., Vitorge, P., 1996. Migration of $^{45}$Ca and $^{90}$Sr in a clayey and calcareous sand: calculation of distribution coefficients by ion exchangge theory and validation by column experiments. *J. Contam. Hydrol.* **21**, 175–188.

Lichtner, P., Zachara, J.M., 2005. Modeling batch reactor ion exchange experiments of strontium–calcium–magnesium–potassium–sodium on Hanford Sediments, PNNL-141083P. Pacific Northwest National Laboratory, pp. 100.

Liu, D.-C., Hsu, C.-N., Chuang, C.-L., 1995. Ion-exchange and sorption kinetics of cesium and strontium in soils. *Appl. Radiat. Isot.* **46**, 839–846.

Long, P.E., Wood, B.J., 1986. Structures, textures, and cooling histories of Columbia River basalt flows. *Geol. Soc. Am. Bull.* **97**, 1144–1155.

MacKenzie, F.T., Bischoff, W.D., Bishop, F.C., Loijens, M., Schoonmaker, J., Wollast, R., 1983. Magnesian calcites: Low-temperature occurrence, solubility, ans solid-solution behavior. In: Reeder, R.J. (Ed.), *Carbonates: Mineralogy and Chemistry; Reviews in Mineralogy.* Mineralogical Society of America, pp. 97–144, vol. 11.

Magaritz, M., Brenner, I.B., Ronen, D., 1990. Ba and Sr distribution at the water-table: implications for monitoring ground-water at nuclear waste repository sites. *Appl. Geochem.* **5**, 555–562.

McKinley, J.P., Rawson, S.A., Horton, D.G., 1986. Form and composition of secondary mineralization in fractures in Columbia River Basalts. In: Chambers, A.D.R.J.a.W.F. (Ed.), *Chambers Microbeam Analysis—1986.* San Francisco Press, Inc., pp. 127–130.

Mucci, A., Morse, J.W., 1983. The incorporation of $Mg^{2+}$ and $Sr^{2+}$ into calcite overgrowths: influences of growth rate and solution composition. *Geochim. Cosmochim. Acta* **47**, 217–233.

Mucci, A., Morse, J.W., 1984. The solubility of calcite in seawater solutions of various magnesium concentration, $I_t = 0.697$ m at 25 °C and one atmosphere total pressure. *Geochim. Cosmochim. Acta* **48**, 815–822.

Naqa, A.E., Kuisi, M.A., 2004. Hydrogeochemical modeling of the water seepages through Tannur Dam, southern Jordan. *Environ. Geol.* **45**, 1087–1100.

OECD, 2002. Chernobyl: assessment of radiological and health impacts, <http://www.nea.fr/html/rp/chernobyl/>. OECD Atomic Nuclear Agency.

Ohnuki, T., Kozai, N., 1994. Sorption characteristics of radioactive cesium and strontium on smectite. *Radiochim. Acta* (66/67), 327–331.

Parkman, R.H., Charnock, J.M., Livens, F.R., Vaughan, D.J., 1998. A study of the interaction of strontium ions in aqueous solution with surfaces of calcite and kaolinite. *Geochim. Cosmochim. Acta* **62**, 1481–1492.

Pinnioja, S., Kamarainen, E., Jaakkola, T., Siitari-Kauppi, M., Muuronen, S., Lindberg, A., 1985. Sorption and diffusion of cobalt, strontium, cesium and americium in natural fissure surfaces and drill core cups studied by autoradiography, I. Nuclear Waste Commission of Finnish Power Companies, pp. 33.

Reeder, R.J., Lamble, G.M., Northrup, P.A., 1999. XAFS study of the coordination and local relaxation around $Co^{2+}$, $Zn^{2+}$, $Pb^{2+}$, and $Ba^{2+}$ trace elements in calcite. *Am. Mineral.* **84**, 1049–1060.

Reidel, S.P., Fecht, K.R., 1994. Geologic Map of the Priest Rapids 1:100,000 Quadrangle, Washington. Open file Report 94-13. Washington Division of Geology and Earth Resources, pp. 22.

Rhoades, J.D., 1996. Salinity: electrical conductivity and total dissolved solids. In: Bigham, J.M. (Ed.), *Methods of Soil Analysis Part 3.* American Society for Agronomy, pp. 417–435.

Riley, R.G., Zachara, J.M., 1992. Chemical Contaminants on DOE Lands and Selection of Contaminant Mixtures for Subsurface Science Research, DOE/ER-0547T. US Department of Energy, pp. 77.

Rimstidt, J.D., Balog, A., Webb, J., 1998. Distribution of trace elements between carbonate minerals and aqueous solutions. *Geochim. Cosmochim. Acta* **62**, 1851–1863.

Serne, R.J., Bjornstad, B.N., Gee, G.W., Schaef, H.T., Lanigan, D.C., McCain, R.G., Lindenmeir, C.W., Orr, R.D., LeGore, V.L., Clayton, R.E., Lindberg, M.J., Kutnyakov, I.V., Baum, S.R., Geiszler, K.N., Valenta, M.M., Vickerman, T.S., Royack, L.J., 2002a. *Characterization of Vadose Zone Sediment: Borehole 299-E33-46 Near B110 in the B BX-BY Waste Management Area, PNNL-14119.* Pacific Northwest National Laboratory, pp. 100..

Serne, R.J., Last, G.V., Gee, G.W., Schaef, H.T., Lanigan, D.C., Lindenmeir, C.W., Lindberg, M.J., Clayton, R.E., LeGore, V.L., Orr, R.D., Kutnyakov, I.V., Baum, S.R., Geiszler, K.N., Brown, C.F., Valenta, M.M., Hill, T.S., 2002b. *Characterization of Vadose Zone Sediment: Borehole 299-E33-45 Near BX-102 in the B-BX-BY Waste Management Area, PNNL-14083.* Pacific Northwest National Laboratory, pp. 100.

Serne, R.J., Jones, T.E., Lindberg, M.J., 2003. *Laboratory Scale Bismuth Phosphate Extraction Process Simulation to Track the Fate of Fission Products, PNNL-14120.* Pacific Northwest National Laboratory, pp. 100.

Smith, C.L., Drever, J.I., 1976. Controls on the chemistry of springs at Teels Marsh, Mineral County, Nevada. *Geochim. Cosmochim. Acta* **40**, 1081–1093.

Spalding, B.P., 1980. Adsorption of radiostrontium by soil treated with alkali metal hydroxides. *Soil Sci. Soc. Am. J.* **44**, 703–709.

Spalding, B.P., 1981 *Precipitation of Radiostrontium in Soil*, vol. 3. Plenum, New York, pp. 243–250.

Sposito, G., 1984. The Surface Chemistry of Soils. Oxford University Press, Oxford.

Sposito, G., 1989. The Chemistry of Soils. Oxford University Press, Oxford.

Strelko, V.V., Mardanenko, V.K., Yatsenko, V.V., Patrilyak, N.M., 1998. Sorption of cesium and strontium on native vermiculite and vermiculite modified with copper ferrocyanide. *Russ. J. Appl. Chem.* **71**, 1746–1749.

Stumm, W., Morgan, J.W., 1996. Aquatic Chemistry. John Wiley, London.

Suksi, S., Kamerainen, E., Jaakkola, T., Ervanne, H., Lindberg, A., 1986. *Sorption and diffusion of cobalt, nickel, strontium, iodine, cesium, and americium in natural fissure surfaces and drill core cups studied by autoradiography, II.* Nuclear Waste Commission of Finnish Power Companies, pp. 35.

Suksi, S., Kamerainen, E., Siitari-Kauppi, M., Lindberg, A., 1987. *Sorption and diffusion of cobalt, nickel, strontium, iodine, cesium and americium in natural fissure surfaces and drill core cups studied by*

*autoradiography, III*. Nuclear Waste Commission of Finnish Power Companies, pp. 69.

Tesoriero, A.J., Pankow, J.F., 1996. Solid solution partitioning of $Sr^{2+}$, $Ba^{2+}$, and $Cd^{2+}$ to calcite. *Geochim. Cosmochim. Acta* **60**, 1053–1063.

USGS, 2001. Alkalinity and Acid Neutralizing Capacity. In National Field Manual for the Collection of Water-Quality Data, http://water.usgs.gov/owq/FiledManual/Chapter6/6.6-contents.html. US Geological Survey.

Vaniman, D.T., Chipera, S.J., 1996. Paleotransport of lanthanides and strontium recorded in calcite compositions from tuffs at Yucca Mountain, Nevada, USA. *Geochim. Cosmochim. Acta* **60**, 4417–4433.

Wogelius, R.A., Fraser, D.G., Wall, G.R., Grime, G.W., 1997. Trace element and isotopic zonation in vein calcite from the Mendip Hills, UK, with spatial-process correlation analysis. *Geochim. Cosmochim. Acta* **61**, 2037–2051.

Xu, N., Hochella Jr., M.F., Brown Jr., G.E., Parks, G.A., 1996. Co(II) sorption at the calcite-water interface: I. X-ray photoelectron spectroscopic study. *Geochim. Cosmochim. Acta* **60**, 2801–2815.

Yamanaka, M., Nakano, T., Tase, N., 2005. Hydrogeochemical evolution of confined groundwater in northeastern Osaka Basin, Japan: estimation of confined groundwater flux based on a cation exchange mass balance method. *Appl. Geochem.* **20**, 295–316.

Yanagi, T., Watanabe, M., Yamamoto, K., 1989. Sorption behavior of cesium and strontium ions on mixtures of clay sorbents. *J. Nucl. Sci. Technol.* **26**, 861–864.

Yasuda, H., Uchida, S., Muramatsu, Y., Yoshida, S., 1995. Sorption of manganese, cobalt, zinc, strontium, and cesium onto agricultural soils: statistical analysis on effects of soil properties. *Water, Air, Soil Pollut.* **83**, 85–96.

Zachara, J.M., Cowan, C.E., Resch, C.T., 1991. Sorption of divalent metals on calcite. *Geochim. Cosmochim. Acta* **55**, 1549–1562.

Zeissler, C.J., Wight, S.A., Lindstrom, R.M., 1998. Detection and characterization of radioactive particles. *Appl. Radiat. Isot.* **49**, 9–11.

Zeissler, C.J., Lindstrom, R.M., McKinley, J.P., 2001. Radioactive particle analysis by digital autoradiography. *J. Radio. Nucl. Chem.* **48**, 407–412.

Zhu, C., Burden, D.S., 2001. Mineralogical compositions of aquifer matrix as necessary initial conditions in reactive contaminant transport models. *J. Contam. Hydrol.* **51**, 145–161.